Theor Chem Acc (2011) 130:609–632
DOI 10.1007/s00214-011-0936-6

REGULAR ARTICLE

Thermo-dynamical contours of electronic-vibrational spectra simulated using the statistical quantum–mechanical methods

Vladimir Pomogaev · Anna Pomogaeva · Pavel Avramov · K. J. Jalkanen · Sergey Kachin

Received: 2 July 2010 / Accepted: 2 April 2011 / Published online: 3 June 2011

Abstract Three polycyclic organic molecules in various solvents focused on thermo-dynamical aspects were theoretically investigated using the recently developed statistical quantum mechanical/classical molecular dynamics method for simulating electronic-vibrational spectra. The absorption bands of estradiol, benzene, and cyanoanthracene have been simulated, and most notably, the increase in the spectral intensity for the lowest excited state transition as the temperature is increased observed experimentally is well reproduced. In addition, this method has been extended to treat luminescent processes also, and it is seen that the experimental emission spectrum of cyanoanthracene is also well described. The method still needs further refinement, but results to date, including those presented in this work, document clearly that our model is one which is able to treat the many complex effects that the environment have on electronic absorption and emission spectra.

Keywords Organic compounds · Molecular dynamics · Photophysical properties · Electronic spectra

Dedicated to Professor Akira Imamura on the occasion of his 77th birthday and published as part of the Imamura Festschrift Issue.

V. Pomogaev (✉) · P. Avramov · S. Kachin
Siberian Federal University, Svobodnyi 79,
660041 Krasnoyarsk, Russia
e-mail: helperv@gmail.com

V. Pomogaev · A. Pomogaeva
Notre Dame Radiation Laboratory, University of Notre Dame,
Notre Dame, IN 46556, USA

P. Avramov
Kirensky Institute of Physics, 660036 Krasnoyarsk, Russia

K. J. Jalkanen
Laboratory of Biomedical Vibrational Spectrscopy,
Institute for Research and Development, Universidade do Vale
do Paraíba, Avenida Shishuma Hifumi, 2911, Urbanova,
São José dos Campos, CEP-12244-000 São Paulo, Brazil

K. J. Jalkanen
Department of Physics, Quantum Protein (QuP) Center,
Technical University of Denmark, 2800 Kgs. Lyngby, Denmark

1 Introduction

It is well known that chemical photophysics methods can be used to treat the problem of identifying, establishing, and characterizing the interdependencies between polyatomic molecular spatial structures of molecules and the molecules' spectral-luminescent properties: electronic transition energies/frequencies, vibrational frequencies, probabilities for both photo-absorption and photo-emission of various energies and polarization states, and also various radiationless processes, for example, intersystem crossing, and both electronic, vibrational, rotational energy and momentum transfer. Clearly a sound theoretical basis is required for one to rigorously analyze these properties, which are required for one to obtain a better understanding of the processes involved, in particular, for organic, bioinorganic and bioorganic molecules, compounds and complexes. Experimental spectral-luminescent parameters extracted from the spectra should be consistent with those derived from theoretical calculations, which in fact can be described more clearly and precisely. Quantum–mechanical (QM) methods are effective tools to study the photophysical and photochemical properties of various compounds [1, 2]. Calculations of electronic excited states using these approaches give single-point energies corresponding to narrow spectral lines. Quantum mechanical and classical mechanical molecular dynamics (QMMD and

CMMD) simulation methods [3–5] can provide alternative and complementary methods for studying the photophysical properties of organic compounds under various thermodynamical (TD) influences and perturbations. Here, one wishes to obtain theoretical spectral profiles that are consistent with those determined experimentally [6].

Theoretical investigations of large polymers and biopolymers with aperiodic sequences of molecular segments are still complicated tasks to perform. Proteins are heteropolymers, so many of the models used are not strictly applicable to these systems. Nature uses 20 amino acids and in many cases one or more of these 20 amino acids in addition are post-transcriptionally modified for the protein to function. In many cases, the protein folds and then is modified before it is active, in extreme cases parts are actually cut out, making the paradigm that the sequence determines the structure and therefore the function not necessarily applicable. Spectroscopy and molecular simulation are ideal tools to monitor such complex biological processes. QM calculations often face serious challenges to provide clear pictures of such complex photophysical processes within systems and between complex coupled systems, such as the transfer or exchange of energy between unbound (not covalently bound) molecules (anthracene–naphthalene complex) [7, 8]. In many cases, the spectral-luminescent properties of molecules are strongly dependent on environmental changes (tryptophan in different solvents) [9, 10]; and the same or different features/properties are strongly dependent on other different TD conditions (cyanoanthracene at high pressures) [11]. In some cases, one can obtain structures from several snapshots taken from either QMMD or CMMD simulations, but a lot of points are needed to describe realistic photoprocesses. In addition, one must make sure that the initially prepared state one is modeling is actually the same one that one is probing experimentally. Instead of treating the many complicated structural modifications separately, there is a more direct and simple way by combining the QM and MD treatments. MD simulations give one an opportunity to consider the interactions of the chosen molecule with external forces and in aqueous solution or other appropriate biological environments. To be able to simulate the spectral properties of flexible molecules, it is necessary to properly sample the changes in time which occur for the individual molecules and also for the variability of the local environment of the molecules or molecular complexes, especially when one is comparing or simulating the results of measurements on a distribution of molecules and not only one molecule or molecular complex. Here, it is necessary to perform the calculations with QM methods, as the transition moments required are not accurate using classical mechanical treatments. Hybrid MD simulations and a series of QM calculations for the system along the reaction path for the process(es) can provide the photophysical spectral parameters for all possible conformers and the probability of occurrence of each structure, both of which are required for simulating the measured molecular spectrum. If one performs structure optimizations for all of the randomly generated starting structures via a Monte Carlo procedure, one could in theory also simulate the measured spectrum. But here one does not necessarily know or determine the transition rates between the various states, and it may be that the barriers are such that during the experiment, one is trapped in a finite number of local minima. In many cases, biological systems are not in thermodynamic equilibrium, and it is important to know the starting structure (conformer) and/or species of the molecular system before one starts to measure and/or simulate the spectra. In many cases, the conformer in the solid crystalline (or amorphous) state, in the so-called liquid crystal, in aqueous solution, in solvents of varying polarity, or in the membrane environment are not the same. For example, for Leu-enkephalin, three different crystal structures have been reported (from three different solvent systems), and it is not obvious that the actual structure in aqueous solution is any of these structures [12]. And when Leu-enkephalin binds to its receptor, there may be additional changes, both in the conformation of Leu-enkephalin itself and in the receptor protein, the so-called induced fit binding [13]. Here, modeling of and measurement of the electronic, vibrational, nuclear magnetic resonance, and inelastic incoherent neutron scattering (IINS) spectroscopies, and some combination of these various techniques/methods, have a lot to offer [14–16]. But more work is required to model the line widths of the experimental spectra, as the complexity is such that one must be able to distinguish the various conformations (stable minima), from fluctuations in the solvent and environment of the species. Here, modeling studies like ours are fundamental for the field to continue to develop, and for one to be able to determine not only the number of conformers present, but the structure of each, similar to what can now be done with both X-ray crystallography and NMR spectroscopy. To date, only the percentage of secondary structural elements has been able to be determined from electronic absorption, electronic circular dichroism (ECD), vibrational absorption (VA), vibrational circular dichroism (VCD), Raman scattering, Raman optical activity (ROA) and IINS spectroscopies and combinations thereof. The long-term goal is a complete structure determination using the combination of both vibrational and electronic absorption and emission spectroscopies, combined also with IINS measurements and modeling studies.

Theoretical approaches to determine electronic and vibrational molecular structures via several quantum–mechanical (QM) methods have been developed and

widely applied due to the recent progress and advances in computer (in silico) technologies, both hardware and software. Currently, the calculation of chemical and photophysical properties can be carried out due to the improvements and developments in advanced program packages like Gaussian [17], the Cambridge Analytical Derivatives Package (CADPAC) [18], the Amsterdam Density Functional (ADF) package [19], Turbomole [20], Dalton Quantum Chemistry Program [21], Accelrys Material Studio with blocks of various programs [22], General Atomic and Molecular Electronic Structure System (GAMESS) [23], SYSMO [24, 25], MOLCAS [26] to name a few of the many currently available quantum chemical packages. This list is not complete, and there are many codes being developed in the condensed matter physics community, for example, Vienna Ab initio Simulation Package (VASP) [27] and Spanish Initiative for Electronic Simulations with Thousands of Atoms (SIESTA) [28], but the later codes do not have the breath of molecular properties which have been implemented in codes like SYSMO and CADPAC, the developments of which have focused on molecular properties and are not limited to energies, gradients and finite difference Hessians and atomic polar tensors (APTs), the latter two required to simulate the VA spectra. Several formalisms/levels of theory, for example, Hartree–Fock–Roothaan–Hall (HFRH) [29, 30], or post-Hartree–Fock methods which treat electron correlation, for example, Møller–Plesset perturbation theory (MP2) [31, 32], coupled cluster theory (CC) [33], several types of multi-configuration self-consistent field (MCSCF) such as complete active space SCF (CASSCF) [2, 33] and complete active space perturbation theory (CASPT2) [34]. In addition to wave function–based quantum mechanical methods [35, 36], density functional theory (DFT) methods based on Kohn and Sham's [1, 2, 37, 38] extension of Thomas [39] and Fermi [40, 41] theories which were extended by Dirac (Thomas–Fermi–Dirac) [42] have also become quite popular and are now implemented in most quantum chemistry packages, including most of those mentioned above. In addition, the CAS method from wave function theory (WFT) has been extended recently to DFT theory with the so-called CAS-DFT method [43, 44]. Finally, there are the ab initio DFT methods of the Bartlett group at the University of Florida in Gainesville [45]. Here, one has used the information and knowledge developed in quantum chemistry to develop more rigorous and first principles exchange and correlation functionals, which are required to accurately calculate molecular properties of molecular complexes and aggregates, including but not limited to both intramolecular and intermolecular hydrogen bonding in biomolecules in aqueous solution [46–48], dispersion/Van der Waals (VdW) forces important in noble gas dimers, benzene dimers and in DNA and RNA base stacking [49–52], infrared intensities [53], VCD intensities [54], Raman scattering intensities [55, 56], ROA intensities [57–59], EA intensities in aqueous solution using an effective fragment model and/or using long-range corrected XC functionals [60–62], ECD intensities [63–65], fluorescence and phosphorescence intensities [66, 67], and finally nuclear magnetic resonance (NMR) shielding and coupling constants [68–72].

In addition, there are the various linear and nonlinear tensor response molecular properties and property surfaces which depend on the electric field, electric field gradient, magnetic field, and magnetic field gradient, both static and frequency dependent, and other tensor quantities: the electric dipole moment, electric dipole–electric dipole polarizability, electric dipole–electric quadrupole polarizability, electric dipole–magnetic dipole polarizability, various hyperpolarizabilities, and the magnetic dipole moment, their transition moments, and finally their derivatives with respect to both nuclear displacements, and nuclear velocities (momenta), the so-called, molecular property surfaces [73]. To be able to simulate all of these properties for both molecules and molecular complexes requires one to perform MD simulations, which can be run using classical, quantum or multi-scale methods [3]. It should be noted that the simple approximate methods very often provide much faster treatments for the calculation/simulation of some of these properties. What is fundamental is to maintain a satisfactory accuracy that is very important if hundreds of calculations are desired and necessary as in the cases presented here.

At the same time, many of the mentioned methods are not feasible for large molecular simulations. Here, the need to make approximations is apparent, but one needs to control and document the errors introduced at each stage/level of approximation. In many cases, by making various approximations, one loses fundamental physics, chemistry, and molecular biology; one fails to predict or be able to reproduce known experimental data [54, 73]. This was in fact the motivation to develop quantum mechanics, the inability of classical mechanics to account for the photoelectric effect and blackbody radiation. In the case of both DFT and WFT forms of quantum mechanics, VdW or dispersion forces are not apparent at the lower levels of approximation, and one must have very accurate treatments of electron correlation, both local and nonlocal electron correlation in DFT and static and dynamic electron correlation in WFT, to get these effects correct for the correct reasons, and not due to some fortuitous cancellation of errors [34, 45, 50].

Currently, there are several modern QM/MD methods used to obtain excited electronic-state absorption profiles [74–87]. Nonadiabatic and adiabatic quantum MD

simulations of an excess electron in water under various TD conditions have been performed to obtain absorption spectra when the hydrated electron is a ubiquitous transient species in irradiated aqueous systems [74–78]. The solvatochromic effect has been studied by using the supermolecule approach with the averaged solvent electrostatic potential (ASEP)/MD method. The initial geometry and charge distribution of the solute and solvent molecules have been determined using the MD simulations, and then the total structure or just the chromophore surrounded by shells of hydrogen-bonded solvent molecules have been re-optimized before calculating the excited electronic-state transition energies and the corresponding oscillator strengths [79–81]. Other approaches for obtaining spectral contours using hybrid QC/MD schemes have been reported in recent years, for example, the use of flexible molecules in simulating vibrations in the electronic spectra of amides and β-ionone [82, 83], the use of effective fragment potentials within QM/MM to simulate solvent effects with TD-DFT methods [84, 85], and finally to employ a full multiple spawning (FMS) method for multistate quantum dynamics using both semi-empirical and ab initio QM methods to treat the effects of complex environments [86]. In addition, the effects of concentration on properties and as a means to increase intensities in liquid water have been investigated using a combined coupled cluster and molecular dynamics method [87].

In contrast to the aforementioned methods, our statistical quantum–mechanical/molecular-dynamic (SQMMD) technique involves MD simulations using fully flexible molecular structures, where the QM calculations for the excited nonequilibrium states are performed in an attempt to reproduce and understand the experimental spectral shapes. Theoretical spectra can be built up from envelopes of statistically averaged intensities of electronic transitions for these nonequilibrium structures weighted by their populations determined by/from the MD simulations. This idea has been shown and documented to apply for organic compounds in solvents under various TD conditions [6].

In order to be sure that there are neither abnormal structural nor photophysical deviations, the following scheme can be applied to achieve a much more precise picture: (a) optimization of the main structure by the most appropriate and accurate QM model, (b) photophysical properties are calculated at a high theoretical level, such as the "gold standard", coupled cluster (CC) theory, and compared with experimental data, (c) appropriate spectral parameters for a semi-empirical HFRH implementation have to be found/derived (parameterization undertaken with a set of both experimental and high level ab initio wave function theory and/or density functional theory data of sufficient accuracy and breadth, the so-called training set) or another similar method could be used (SCC-DFTB [12, 14–16] or PM6 [36]), (d) MD simulation with intermediate QM calculations, and finally (e) the statistical–mechanical averaging needs to be carried out. If it is found to be necessary, it is possible to use local QM/MD simulations to determine the position and number of the solvent molecules in the neighboring environment of the compounds under study, in addition to extending and introducing more flexibility into the simple point charge (SPC) model used for liquid simulations of water [88]. For certain properties, this may be extremely important, for example, when water molecules form a hydrogen bonded network(s) which stabilizes a conformer and/or species of a molecule (zwitterionic state of amino acids) which are/is not stable without the solvent molecules being present [46, 47, 57–59, 89, 90].

In the present work, thermal profiles of electronic–vibrational (vibronic) absorption and fluorescence spectra are treated and described. Simultaneous electronic and vibrational transitions are known as vibronic transitions. Since the term of vibronic is used mostly for calculating separated exact vibrations of equilibrated molecules, while the statistical method involves an average over an ensemble of vibrations in nonequilibrium structures (conformers) obtained during MD simulation, it would be better to distinguish the term vibronic for the specific cases in which it is used. Here, to include the main features of our method, we use the term active quasi-vibronic (AQV). The "active" is added because we calculate all the transitions and only include those with significant intensities; the "quasi-" is added to signify the averaging. At any rate, the understanding/use of "vibronic" for transitions from the vibrational states of the ground electronic state to vibrational states of electronically excited states still remains.

The statistical absorption spectra between 240 and 320 nm for estradiol in ethanol, hexane, or dimethyl sulfoxide (DMSO) solvents were considered. The dependence of the first electronic band in benzene surrounded by cyclohexane molecules on temperature is described. A transition between the ground state and the lowest singlet excited energy level is forbidden by symmetry for the equilibrium structure, but according to several experimental measurements, spectral intensity for the corresponding band is observed. Finally, both absorption and emission spectra of cyanoanthracene were constructed/simulated. All simulations have been compared with the appropriate and analogous experimental data in the literature.

2 Methodology and computational details

2.1 Various approaches and applications

Absorption and emission spectra due to electronic transitions involve the ground and excited electronic states and

their corresponding vibrational state manifolds, the so-called vibronic states in the molecules. In order to study the spectral-luminescent properties, statistical methods to model electronic spectra were employed [6]. The main features of these methods should be briefly described.

First, in many cases, it is assumed that during a long MD simulation, the molecule is sampling all (or least many) of its possible conformers (conformational states), including undergoing various nuclear vibrations and rotations of the various conformers populated during the TD run. The MD simulation is an attempt to model the environmental conditions which includes temperature, but which in many purely QM simulations are not taken into account. In the MD case, vibrations do not need to be determined explicitly, as well as other displacements: rotations and translations. To obtain the corresponding vibronic spectrum, or as it was redefined for AQV spectrum, one assumes/hypothesizes that the structural deviations and motions in this approach are accurately and correctly determined by the internal molecular and external environmental classical-, quantum–mechanical, or hybrid set of force-field parameters one is using [2–4, 6, 77–94]. The accuracy of the MD trajectories is very important along with the accuracy of the subsequent electronic transition energies, moments, and corresponding oscillator strengths. These accuracies are determined by the choice of the force field, semi-empirical method, or WFT or DFT method used. In the case of ab initio Born–Oppenheimer MD simulations, one has recently attempted to develop so-called linear scaling methods, Car-Parrinello and QM/MM methods to allow one to treat the environment explicitly and in an efficient manner which would allow one to simulate larger biological model systems [91–94]. In addition to having an accurate method to calculate the electronic excited-state energies and their corresponding transition moments, one needs an accurate and efficient method to take into account the environment, solvent, protein, and/or membrane. Clearly one cannot include the complete environment and whole system at the highest level of theory for the MD simulation. But one must somehow benchmark the accuracy of the structures which one will then use in the subsequent higher-level calculations of the excited electronic-state energies and transition moments. In addition, how large should the system be which one needs to use for these calculations. Is it sufficient to only use the structures of the solute, or should one include the first solvation shell in aqueous solution, and all residues or lipids within a certain cutoff distance in the case of a protein or lipid environment, or is it feasible to use just a continuum solvent/environment treatment. These are fundamental questions, all of which are topics for research projects. Some of these questions have been addressed for either vibrational spectral simulations or excited electronic-state energy calculations, but none have been systematically and completely answered to an extent that the research community considers this area of research solved.

Spectral features of the vibrational and electronic linewidths can be studied separately, applying, for instance, a density of states (DOS) analysis, which will be the focus of a subsequent follow-up work by us. We should like to now note the main differences of our current work from previous investigations. Most of aforementioned techniques [76–81, 87, 89, 90] dealt with the spectral properties and features of rigid molecules in equilibrated systems: equilibrated solute–aqueous solvent configurations or droplets extracted from larger bulk systems and obtained by various methods and/or combinations of MD simulations and geometry optimizations. Several molecules including water [76, 78, 87], formaldehyde [77], acrolein [79, 80], formamide [82], and acetone [84, 85]; and the relatively middle-sized benzophenone [81], coumarin 151 [85], or chromophores as *p*-hydroxybenzylidene-imidazolinone (HBI), 4-Hydroxybenzylidene-1,2-dimethylimidazolinone (HBDI), and, the anionic form of *p*-hydroxybenzylidene acetone (pCK-) [86] in liquid solvents were treated. An implicit ethanol solvent was utilized to calculate isomers of ionone [83]. Different structures and various numbers of hydration shells were used to describe the solvatochromic effects that strongly depend on the aqueous environment. The protonic and polar properties of the aqueous solution noticeably change as evidenced/seen in the molecular spectral properties of the aggregate system. In some cases, the changes in the properties are due to the fact that both the species and conformer of the solute are fundamentally different in an aqueous environment than they are in either the gas phase, in the isolated state in non-polar solvents, or in a nonpolar membrane type environment. One must first have the correct species, structures (conformers), and aggregation states before one can contemplate calculating/simulating various molecular properties, including both the vibrational and electronic absorption and emissions spectra.

In a recent simulation of the vibrational spectra (VA, VCD, Raman, and ROA) of L-alanine and the alanine dipeptide (*N*-acetyl L-alanine *N*′-methyl amide) in aqueous solution, the solute was encapsulated in a hydration shell [89], which was then minimized. The VA, VCD, Raman, and ROA spectra were then calculated using the so-called mechanical harmonic approximation for the structure of the droplet. The structure of the hydrated complex had been optimized. The droplets are obtained from several steps of the MD simulations [90]. The initial system is obtained from a classical MM/MD simulation, which is then used as a starting system for Born–Oppenheimer quantum mechanical molecular dynamics (QM/MD) simulation using the PBE generalized gradient approximation (GGA) DFT level of theory to determine the positions of the

hydration shell surrounding the solute molecules (the L-alanine zwitterion). For the vibrational simulations, the hydrated L-alanine zwitterion was then embedded within bulk water and treated using the PCM continuum solvent model to treat the effects of bulk water. This methodology seems to be optimal for obtaining a finite number of various oscillating conformers for this solute molecule or a solute–solvent droplet and for biomolecules in aqueous solution in general. Obviously, this way gives more accurate molecular structures obtained from Born–Oppenheimer DFT MD simulation trajectories, but it is computationally very expensive for large biomolecular molecules which are very flexible, as are the molecules studied in this work. It would be interesting to compare the aforementioned approach used for simulating the vibrational spectra of biomolecules with the approaches under current discussion and investigation by us in simulating the spectra of photonic transitions in large flexible molecules.

Concerning radiationless vibrational transitions, several other methods can be mentioned where in a similar manner, the matter of vibronic transitions in organic compounds has been considered [95–97]. All these works deal with several exact vibrational modes of specific structures, and they have focused on correctly reproducing several of the most probable/frequent mechanisms accessible for radiationless transitions. Two works [95, 96] use some fitted "molecular parameters" and the last one [97] utilized a combination of first principle calculations with multimode vibronic theory.

In the case of the SQMMD method, nonequilibrium conformers (isolated individual, solvated by a number of nearest molecules, or using an implicitly mimicked environment) obtained from MD trajectories are extracted and used to calculate the energy states and transition probabilities, similarly as was done in [82–85], where the excited-state energies of formamide or acetone using an explicit model of the aqueous solution or ionone using an implicit ethanol solvent model and their corresponding intensities were plotted on the two axes. In order to obtain more realistic spectra which would reproduce the experimental spectra within experimental error and/or instrumental frequency resolution, it is necessary to apply statistical mechanical averaging to take into account, for example, concentration effects, conformational and solvent substates and fluctuations [87]. Our aim was to avoid the problem of and the need to determine the several exact active vibrational modes responsible for a transition (or transitions) that is (are) always specific, new, and unique for each molecule or molecular complex, and require a complete normal mode calculation for the complete system. Another compound or molecular complex requires a new investigation for a new specific set of vibrations (normal modes). This work is expensive in terms of both human and computer resources. Our method is more straightforward, easy and more universal, but it does lead to a loss of accuracy. On the other hand, the idea is to give a qualitative picture that should reflect the main features of the experimentally measured spectra, including the experimental line widths. The initial work [6] concerned the theoretical basis of the SQMMD method regarding absorption processes. Several successful examples of transitions to numerous excited states in the protein structure of tryptophan-cage mini protein (trp cage-mp) and in the estradiol molecule in ethanol at the room temperature were presented. Here, we have extended that work to now obtain fluorescence spectral profiles, thermal broadening spectra under different pressures in various solvents, and the increase in intensity of forbidden transitions in benzene as the temperature is increased.

2.2 Theoretical background

According to the Franck–Condon (FC) principle (approximation), an electronic transition occurs within a stationary nuclear framework during the actual vertical transition [1]. An initial vibrational sublevel of an electronic state is defined by the Boltzmann's distribution $p_i = p\times \exp(-E_i/kT)$, where $E_i = i\times\omega_i$, i and ω_i are the quantum number for the ith vibrational state and its corresponding frequency, respectively. At room temperature and lower, $kT < 210\ \mathrm{cm}^{-1}$, and molecules with the frequencies/modes with $\omega_i > 1{,}000\ \mathrm{cm}^{-1}$ are only in their ground vibrational state, that is, $i = 0$. The lowest vibrational state corresponds to $i = 0$, that is the most probable at or near $T = 0$. For most electronic excited-state calculations, it is accepted as a general rule that most of the molecules are only in their ground vibrational state, and this is the methodology use in most QM calculations of electronic transitions. But for large flexible biomolecules like proteins and peptides, there may be many low-frequency vibrational states which are populated $i > 0$ at room temperature. In such cases, the Franck–Condon overlaps should be calculated for the $i > 0$ states involving these vibrations. But this would also involve anharmonic contributions, as these very low-frequency modes have been shown to be very anharmonic. Hence, the Franck–Condon approximation and the methodology which involves calculating all of the Franck–Condon factors for both the ground and excited electronic states for large flexible biomolecules in a strongly interacting hydrogen bonding solvent very fast become intractable.

Hence, in many cases, one assumes that photo-absorption or photo-emission proceeds from the zeroth vibrational levels of the ground or excited states to the most probable vibrational sublevels of the other electronic state $E_{|0,0\rangle} \rightarrow E_{|n,k\rangle}$ or $E_{|0,t\rangle} \leftarrow E_{|n,0\rangle}$ (Fig. 1). Configuration interaction (CI), time-dependent (TD) Hartree–Fock, CASSCF, CASPT2, CASPT3, CASDFT, MCSCF, and other methods in the framework of ab initio WFT, DFT, or semi-empirical

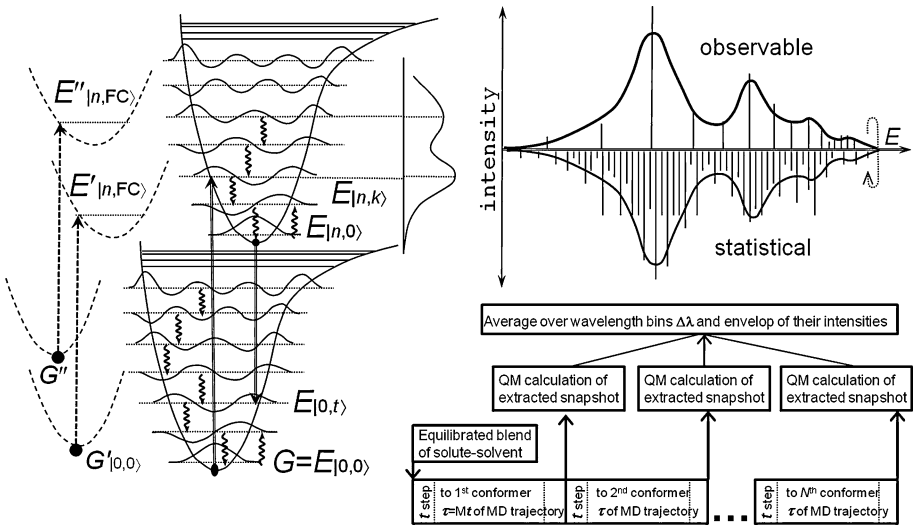

Fig. 1 Schematic photo-transitions in a relaxed system according to the Franck–Condon principle and most probable photo-absorptions ($G' \rightarrow E'$, $G'' \rightarrow E''$) in nonequilibrated conformers are on the left side as well as there is a graphical representation of SQMMD method to reproduce a realistic electron-vibrational spectrum and a flow chart of computational process

WFT or DFT approaches are used to calculate the energies of ground and excited states which are formed according to the so-called frozen orbital approximation from the same molecular orbitals (MOs) determined for the ground state equilibrated structure. But others have treated electronic states corresponding to FC vibrational modes of/from the equilibrium structures of excited energies. In the case of fluorescence, the geometry of the molecule in the excited electronic state relaxes, and there is a red shift due to the energy being less. Some spectroscopic oriented semi-empirical methods such as Zerner's Intermediate Neglect of Differential Overlap (ZINDO) [98] and INDO/sp with a special parameterization implemented in a developmental version of the GAMESS [6] attempt to provide correct transitions to FC states where the multi-center Columbic and exchange integrals are determined by fitting to spectroscopic data. The main idea of the SQMMD method is to reproduce a real "observable" spectrum measured experimentally and/or simulated by some more rigorous and accurate theoretical methods. Here, we produce a "statistical" curve that averages intensities of the radiative transitions (for instance, photo-absorptions $G' \rightarrow E'$, $G'' \rightarrow E''$, and so on) for all possible distorted conformers of the molecular structure under study (Fig. 1).

With regard to our previous work [6], rather than using the desired all vibration approach described above, the frozen orbital approximation has been assumed and used where the atoms remain frozen while the transition proceeds between the electronic ground and excited states due to photo-absorption or between the excited electronic states and either lower electronic states or the ground electronic state due to photo-emission. Translational motions, vibrations, and rotations of the solute molecule appearing along a MD trajectory simulated under some TD conditions are all involved in collisions with solvent molecules. These events are much slower than the events involved in the changing of the states of the electron cloud which occur during the radiation-induced transitions. The Franck–Condon and Born–Oppenheimer approximations allow the states and probabilities (transition rate constants) for the electronic transitions between them to be calculated for each conformer in a transparent manner (see the flow chart in the lower-right corner of Fig. 1). Since the MD time-step for the simulation is extremely short even compared with electronic transitions and vibrations, an average over an energy bin 'frequency resolution' was applied to find the main values of the energies and transition probabilities in this time interval. It should also be noted that even if one assumes that each transition for each conformer (conformation) has a broadening described by one of the commonly used distribution functions (Lorentzian, Gaussian or others) in the same manner used in many other simulations in which the authors use of the spectral linewidth as a free parameter to reproduce the experimental spectra obtained from a set of excited states of an isolated relaxed molecule, a statistical curve determines the actual spectral profile by enveloping just the peaks of (tight suited) vertical excitation energy bands for the fluctuating structures or even their representative averages over energy bins, and this shape is independent of the form of the distribution used for any individual transition. As the actual experimental linewidths and spectral profiles have many contributions, it is very important to understand the various mechanisms, and the contribution of each to the observed experimental linewidth. We assume that a major contribution to the linewidths is due to structural variations during both the absorption and emission processes. We model these fluctuations by our MD simulations. Each so-called vertical transition makes a contribution to the spectral shape/profile where the more-intense transitions mask the less-intense

ones. Configuration interaction singles (CIS) based on INDO/sp is used to obtain the most probable transitions into FC states.

All the aforementioned statements and approaches described above should be expressed in mathematically rigorous and concise equations for better understanding of the theoretical level. We introduce no new sophisticated mathematical tricks, but use the standard text book formulations [1], which are slightly modified to reflect the separate and distinct physical nature of the variables we have chosen.

First of all, the total Hamiltonian H as well as wavefunctions Ψ_n are separated into time-dependent and independent parts within perturbation theory as

$$H = H^{(0)} + H^{(1)}(t) = H^{(0)} + 2H^{(1)}\cos\omega t$$

and

$$\Psi_n(t) = \psi_n \exp(-iE_n t/\hbar),$$

where a solution of the equation $H\Psi = i\hbar\partial\Psi/\partial t$ can be decomposed into a stationary state solution, independent of time, $H^{(0)}\psi_n = E_n\psi_n$ and a time-dependent solution, evolving in time t with a dependency on the angular frequency of the time-dependent perturbation, the radiation field, ω. A simple two-state system with energies E_1 and E_2 in the presence of the perturbation $H^{(1)}(t)$ can be expressed as a linear combination of the basic functions $\Psi(t) = a_1(t)\Psi_1(t) + a_2(t)\Psi_2(t)$. Substituting this function into the total Hamiltonian and solving the obtained equation [1], one can arrive at the explicit forms for the coefficients $a_1(t) = \left\{\cos\Omega t + \frac{i\omega_{21}}{2\Omega}\sin\Omega t\right\}e^{-\frac{1}{2}\omega_{21}t}$ and $a_2(t) = -\left(\frac{i|V|}{\Omega}\right)\sin\Omega t e^{\frac{1}{2}\omega_{21}t}$, where $\hbar\omega_{21} = E_2 - E_1, \Omega = \frac{1}{2}\left(\omega_{21}^2 + 4|V|^2\right)^{\frac{1}{2}}$ and the operator V is defined from the off diagonal matrix elements (ME) for the case of constant perturbation $\langle 1|H^{(1)}(t)|2\rangle \equiv H_{12}^{(1)}(t) = \hbar V_{12}$ and $H_{21}^{(1)}(t) = \hbar V_{21}^*$. The probability of finding the system in one of these states as a function of time is $P_i(t) = |a_i(t)|^2$, where $i = 1$ or 2. Taking into account that the perturbation slowly induces the *initial* state to reach its *final* state, and that the initial and final states can be either the ground or excited state, an equilibrium is finally reached when the populations of states became steady. The probability can then be assumed to be time independent $P_f = \omega_{fi}^{-2}\left|V_{fi}\right|^2$.

For a general many-level system, the transition rates $k = \mathrm{d}P/\mathrm{d}t$ are the changes in the probabilities of being in initial states, and the intensities of the spectral lines are proportional to these transition rates. They depend on the rate of transfer of energy between the system and electromagnetic field. It follows that, at resonance, Fermi's golden rule $k = 2\pi\hbar\left|V_{fi}\right|^2\rho\left(E_{fi}\right)$ can be used. It asserts that to calculate a transition rate, all we need do is to multiply the square modulus of the transition matrix element V between the two states by the density of states at the transition frequency, where $\rho(E)\Delta E$ is defined as the number of states in the range E to $E + \Delta E$. The central problem is to define the types of transition operators V and how they depend on the wavefunctions (in WFT) and/or on the density (in DFT). The transition operators are constructed according to QM or QC phenomena that the molecules are expected to experience (come under the influence of), such as absorption, emission, collisions, vibrational energy transfer, and singlet–triplet transitions via intersystem crossing type mechanisms, among others. The most intense transitions are induced by the interaction of the electric component of the electromagnetic field with the electric dipole associated with the transition. The intensity of the transition is proportional to the square of the electric dipole transition moment $\mu_{fi} = \langle f|\mu|i\rangle$ (the electric dipole moment operator is a vector).

Usually one works within the Born–Oppenheimer adiabatic approximation, and then an electronic transition occurs within the stationary nuclear state framework. As a result, the nuclear positions remain unchanged during the actual transition, but then readjust once the electrons have adopted their final distribution in the excited electronic stationary state. This approximation allows one to separate the task into electronic and nuclear parts and to solve them independently $\psi_{in} = \phi_i(\mathbf{r},\mathbf{R})\rho_{in}(\mathbf{R}) \equiv |i\{n\}\rangle$, where $\mathbf{r}$ and $\mathbf{R}$ denote the electronic and nuclear coordinates, respectively. The electronic wavefunction depends parametrically on the nuclear coordinates. Molecular electronic transitions occur from (start in) the ground vibrational state of the lowest electronic state $|\phi\rho\rangle$ and end in the vibrational state that it most resembles (has largest vibrational overlap) in the upper excited electronic state $|\phi'\rho'\rangle$. In this way, the vibrational wavefunction undergoes the least change, which corresponds to the preservation of the dynamical state of the nuclei as required by the FC principle. Classically, the transition occurs when the internuclear separation is equal to the equilibrium bond length of the lower electronic state that sometimes is called the Condon simplification $R = R_0$, but this is not necessary condition.

In a molecule, the electric dipole moment operator depends on the positions and charges of the electrons as well as the nuclei $\mu = -e\sum_i \mathbf{r_i} + e\sum_s Z_s\mathbf{R_s} = \mu_e + \mu_N$

The electric dipole transition moment is therefore

$$\begin{aligned}\langle\phi'\rho'|\boldsymbol{\mu}|\phi\rho\rangle &= \langle\phi'(\mathbf{r},\bar{\mathbf{R}})\rho'(\mathbf{R})|\boldsymbol{\mu}_e + \boldsymbol{\mu}_N|\phi(\mathbf{r},\bar{\mathbf{R}})\rho(\mathbf{R})\rangle \\ &= \langle\rho'(\mathbf{R}) \mid \rho(\mathbf{R})\rangle\langle\phi'(\mathbf{r},\bar{\mathbf{R}})|\boldsymbol{\mu}_e|\phi(\mathbf{r},\bar{\mathbf{R}})\rangle \\ &\quad + \langle\phi'(\mathbf{r},\bar{\mathbf{R}}) \mid \phi(\mathbf{r},\bar{\mathbf{R}})\rangle\langle\rho'(\mathbf{R})|\boldsymbol{\mu}_N|\rho(\mathbf{R})\rangle = \mu_{\phi'\phi}S(\rho',\rho).\end{aligned}$$

The integral over the electron coordinates is zero $\langle\phi'|\phi\rangle = 0$ because the electronic states are assumed to be orthogonal to one another for each selected value of $\mathbf{R}$.

To a reasonable first approximation, the transition due to the electric dipole moment is independent of the locations of the nuclei so long as they are not displaced by a large amount from equilibrium, and so the integral may be approximated by a constant $\mu_{\phi'\phi}$. $S(\rho'\rho)$ is the overlap integral between the two vibrational states in their respective electronic states. The electric dipole transition moment is therefore largest between vibrational states that have the greatest overlap. If one assumes that nuclear wavefunctions are orthogonalized and normalized, then for the same or for very similar geometrical structures (and corresponding electronic potential energy surfaces (PESs), assuming here also that the PESs are very similar) corresponding to the ground and excited electronic states, the wavefunction of the vibrational sublevel of the ground electronic state and that of the Frank–Condon vibrational sublevel of the excited electronic state should be identical, or at least very similar, leading to $S(\rho\rho) = 1$, and $S(\rho'\rho) = 0$, for $\rho' \neq \rho$. This leads to $\langle\phi'\rho'|\boldsymbol{\mu}|\phi\rho\rangle = S(\rho',\rho)\langle\phi'(\mathbf{r},\bar{\mathbf{R}})|\boldsymbol{\mu}_e|\phi(\mathbf{r},\bar{\mathbf{R}})\rangle = \mu_{\phi'\phi}$ which is then zero if $\rho' \neq \rho$ for FC electronic transitions for both photoabsorption and photoemission. Of course, if the ground and excited electronic-state PESs are very different, this will not apply. Transitions can then occur into a larger number of vibronic states pertaining to the same geometrical molecular structure, where the mutual overlap integrals may or may not be equal to unity. But for the particular case where the PESs are either the same or very similar, there is allowed excitation to only one vibronic level, which is the condition for a very narrow linewidth for the excitation or emission band. Here, only one narrow band is needed for each transition that occurs from the ground electronic state to the excited electronic state (in question). In our case, since we have an ensemble of structures, we have an ensemble of transition energies and hence bands, each of which has its own intrinsic linewidth. The linewidths of these individual transitions also need to be determined. These linewidths are determined by the experimental conditions, temperature, pressure and the nature of the interactions between the solvent/environment and the solute molecules.

The usual way is to solve the vibrational task when electronic energies ε_i are obtained due to separating electron from nuclear motions.

$$\begin{cases} [\mathbf{T_r} + \mathbf{U}(r,r') + \mathbf{U}(r,\bar{R})]\phi_i(r,\bar{R}) = \varepsilon_i(\bar{R})\phi_i(r,\bar{R}) \\ [\mathbf{T_R} + \varepsilon_i(\bar{R}) - E_n]\rho_{in}(R) = \sum_{ii'} \boldsymbol{\Omega}_{ii'}\rho_{in}(R) \end{cases},$$

where $\mathbf{T_r}$ and $\mathbf{T_R}$ are the electronic and nuclear kinetic operators; $\mathbf{U}(r,r')$ and $\mathbf{U}(r,\bar{R})$ are operators of potential electron–electron and electron–nuclear interactions, respectively; the potential coupling between them, and the nonadiabatic operator in the so-called harmonic approximation $\boldsymbol{\Omega}_{ii'} = \sum_\alpha \frac{1}{M_\alpha}\langle\phi_i|\partial/\partial R_\alpha|\phi_{i'}\rangle(\partial/\partial R_\alpha) - \langle\phi_i|T_R|\phi_{i'}\rangle$ can be neglected in the BO approximation because of the vanishing ME of this operator compared with the differences between electronic states, which is true for the lowest levels [1]. According to this system of independent equations, a number of nuclear motion (vibrational) states denoted by n correspond to each ith electronic state. Neither the electronic nor the vibrational wavefunctions depend on time in the time-independent QM calculations. These states are defined by a set of energy levels (or surfaces) by different ways and, perhaps except for several of the simplest small molecules, every molecular system requires an individual treatment based on known group vibrations, symmetries, and other known and experimentally observed properties of the nuclear motions. In many cases, the nature of the vibrational modes and the infrared and Raman activity (selection rules) are determined by group theoretical arguments.

Alternative methods can be and have been utilized to define the changing nuclear positions (vibrational motions), the first of which is to solve the equations of nuclear motion together with the corresponding electronic Schrodinger equation as a function of the nuclear displacements (which actually defines both the ground and excited electronic state potential energy surfaces). Let us consider a system of molecular compounds in an environment using both classical and quantum mechanics where the $q(R,\xi)$ in the Lagrangian $\mathbf{L}$ are the generalized coordinates of solute R and solvent ξ molecules, though ξ can be defined in either explicit or/and implicit manners as well as to include quantum corrections for motions of the atoms in a separated volume.

$$\begin{cases} \mathbf{L} = \frac{1}{2}\sum_\alpha m_\alpha \dot{R}_\alpha^2 + \frac{1}{2}\sum_\beta m_\beta \dot{\xi}_\beta^2 - \sum_{\alpha>\alpha'} V(R_\alpha - R_{\alpha'}) - \sum_{\beta>\beta'} V(\xi_\beta - \xi_{\beta'}) - \sum_{\alpha>\beta} V(R_\alpha - \xi_\beta) \\ \mathbf{H}\phi_i(r,\bar{R}) = \left(-\frac{\hbar^2}{2m}\sum_i \Delta_{r_i} + \sum_{i>i'}\frac{e^2}{|r_i - r_{i'}|} - \sum_{i,\alpha}\frac{z_\alpha e^2}{r_i - \bar{R}_\alpha}\right)\phi_i(r,\bar{R}) = \varepsilon_i(\bar{R})\phi_i(r,\bar{R}) \end{cases}$$

In the simplest method, one uses explicit classical mechanics equations of motion. Here, the electronic Hamiltonian of the solute molecule depends on electronic coordinates r and parametrically on the atomic (nuclear) positions R. The nuclear coordinates are shifted/changed/updated during the MD simulation using the equation of motion. Here, one must either determine the ground and/or excited electronic-state potential energy surfaces on the fly using either WFT, DFT, or semi-empirical approximations to the WFT or DFT, or use a parameterized molecular mechanics force field. Here, one assumes that the shape of the electron orbitals (clouds) change immediately within the adiabatic approximation for nuclear and electronic motions. Naturally calculation of the electronic wave function in WFT or the electron density in DFT should follow immediately after the atomic (nuclear motions) part. Moreover, the electronic wave function in WFT and the Kohn–Sham orbitals in DFT depend parametrically on the

nuclear coordinates. After one has solved for either the electronic wave function or the Kohn–Sham orbitals, one can calculate a variety of different molecular properties, which can then be averaged and compared with the corresponding experimentally observed quantities. One of the postulates of WFT is that for each observable there is a corresponding Hermetian operator which can be evaluated if the electronic wave function is known. For DFT, one must of course reformulate these expressions in terms of the electron density, similar to what needed to be done for the electron kinetic energy, in the original Kohn–Sham paper.

In order to separate and express two different processes, the time-dependent wave function can be separated into *fast* (τ of electron transitions) and *slow* (*t nuclear motion including vibrations*) parts, which are responsible for the electronic transitions and the $\Psi(R,r,t,\tau)=\psi(R,r,t)\exp^{i(\mathbf{k}\cdot\mathbf{r}-\omega\tau)}$, where $R(t,\tau)\ \ +\Delta R=R(t,\tau+\Delta\tau)$, but $R(t)+\Delta R=R(t+\Delta t)$ nuclear motions, respectively. The time-dependent equation in the general sense of electron transitions is solved in the usual manner as described above, but the stationary part can be rewritten in the following form $\mathbf{H}\psi_{in(t)}(r,R)=E_{in(t)}\psi_{in(t)}(r,R)$. The wave function can correspondingly be expressed as $\psi_{in}=\phi_i(r,\bar{R})\rho_{in(t)}(R)\equiv|i\{n(t)\}\rangle$, where the vibration n depends on the time t for the *slow* process. The stationary Schrödinger's equation is time independent only in the sense that the electronic motion depends parametrically on the nuclear coordinates, but nuclei themselves move as a function of time. Molecular wave functions can be defined as combinations of Slater's determinants of molecular orbitals (MOs) with antiparallel spins, φ_l and $\bar{\varphi}_{k'}$, that in general form for CIS that are expressed as

$$\Phi_{lk'}=\left|\varphi_l(1)\bar{\varphi}_l(2)\ldots\frac{1}{\sqrt{2}}\big(\varphi_l(2i-1)\bar{\varphi}_{k'}(2i)+\varphi_{k'}(2i-1)\bar{\varphi}_l(2i)\big)\ldots\varphi_n(2n-1)\bar{\varphi}_n(2n)\right|$$

and a state of the system can be defined through/with these determinants

$$\phi_i=\sum_p A_p\Phi_p=A_0\Phi_0+\sum_{lk'}{}^{\lambda}A_{lk'}{}^{\lambda}\Phi_{lk'}\equiv A_0\Phi_0+\sum_{lk'}{}^{\lambda}A_{lk'}{}^{\lambda}|l\to k'\rangle,$$

where the sign λ denotes types of states (singlet, S_i or triplet T_i), while the symbols l and k' denote occupied and vacant MOs, respectively. For the molecule to be in the ground electronic state requires that all electrons populate (be in) the lowest MOs $\phi_0=\Phi_0$.

The equations of motion provide a route to the nuclear vibrations and a system of equations to define the vibronic states can be presented/given in the following form

$$\begin{cases}\Delta R_\alpha=\dot{R}_\alpha\Delta t+\frac{1}{2}\ddot{R}_\alpha\Delta t^2;\ \text{where time resolution}\\ \Delta t=\int_{\Delta t_k}^{\Delta t_{k+1}}\mathrm{d}t,\quad {}^{\Delta}\bar{R}_\alpha=\bar{R}_\alpha+\Delta R_\alpha;\\ \mathbf{H}\phi_i=\left(-\frac{\hbar^2}{2m}\sum_i\Delta_{r_i}+\sum_{i>i'}\frac{e^2}{|r_i-r_{i'}|}-\sum_{i,\alpha}\frac{\mathrm{z}_\alpha e^2}{|r_i-{}^{\Delta}\bar{R}_\alpha|}\right)\\ \phi_i\big(r,{}^{\Delta}\bar{R}\big)=\varepsilon_i\big({}^{\Delta}\bar{R}\big)\phi_i\big(r,{}^{\Delta}\bar{R}\big),\\ \text{where the excited state wavefunction is given by}\\ \phi_p\big(r,{}^{\Delta}\bar{R}\big)=\sum_{(ik)}A_{ik,p}\Phi_{ik}\big(r,{}^{\Delta}\bar{R}\big).\end{cases}$$

where first equation of this system represents motion of nuclei α with coordinates R_α and time interval Δt which define their displacement ΔR_α and spatial structure of snapshot conformers, but updated coordinates provide geometrical parameters ${}^{\Delta}\bar{R}_\alpha$ for electronic wavefunctions ϕ_i or ϕ_p included into Hamiltonian $\mathbf{H}$ and third equation for calculating excited states. It needs to be pointed out that the molecular wavefunctions are represented in terms of molecular orbitals which are themselves represented as linear combinations of atomic orbitals (MO LCAO) $\phi_i\equiv|i\rangle=\sum_\mu^m c_{\mu i}\chi_\mu$ and the squares of these coefficients define the localization of MOs on corresponding AOs (which are normally, but not always, centered on individual nuclei).

The stereochemical structures, energy states, and photophysical properties of N conformers are obtained from snapshots of the fluctuating molecule during an MD simulation (taken every time-step after each Δt interval). The transition energies are calculated for all of the structures extracted from the MD simulation. The effective spectral width in frequency units is defined as the frequency interval between the highest and lowest transition energies and is divided into wavelength intervals $\Delta\lambda$. In the experiments, the frequency resolution Δv depends on both the instrument and the experimental conditions. For each individual transition, the spectral linewidth is determined by the lifetime of the molecule in the excited vibronic state, which depends on a variety of physical conditions, for example, temperature, pressure, solvent in solution, buffer gas in the gas phase, and interactions with other molecules and the lattice in the crystalline state. Absorption and fluorescence intensities for each conformer correspond to their oscillator strengths f for electric dipole allowed transitions, the mechanism which we consider in this work. The method is assumed to apply to various phases (gas, solution, and in solid state) under different TD conditions in a broad range of temperatures, pressures, concentrations and also environments (solvents, buffer gases, and other

molecules/species or even impurities in the crystalline environment). It should be noted that various effects and broadening mechanisms appearing due to interaction of solute and solvent can be included to a final spectral curve implicitly.

An averaged band intensity on $\Delta\lambda$ bin is defined through the relative absorptivity $\varepsilon_{\Delta\lambda} = p_{\Delta\lambda} f_{\Delta\lambda}$, where $p_{\Delta\lambda} = N_{\Delta\lambda}/N$ is the probability to find an excited state of the oscillating molecule in this energy interval. The oscillator strength $f_{\Delta\lambda}$ is an averaged value, and $N_{\Delta\lambda}$ is the number of conformers that provide energy transitions within the $\Delta\lambda$ interval [6]. Finally, a statistical spectrum is constructed as an envelope over these intensities.

The method can also be extended to treat fluorescence as follows. The relative absorption (or emission) intensities can be estimated as a product of probabilities $I_{\Delta\lambda} = p_{\Delta\lambda} \cdot k_r \cdot \gamma_{\Delta\lambda} = \left[p_{\Delta\lambda} \cdot k_r \cdot k_r / \left(k_r + \sum k_{pf}\right)\right]$. The averaged fluorescence quantum yield $\gamma_{\Delta\lambda}$ is inversely proportional to the mean values of the radiative rate constants k_r and the sum of the transition probabilities of all photoprocesses proceeding from the same state. For each configuration the quantum yield is $\gamma_{\Delta\lambda} = k_r / \left(k_r + \sum k_{pf}\right)$, where k_{pf} are the electronic radiationless transition rates. In the cyanoanthracene cases, S_1 has a fluorescence quantum yield (unitless quantity) that depends only on k_r and the rate of cross-section (singlet–triplet) conversion $\sum k_{1f} \approx k_{ST}$ [99, 100].

2.3 Technical details of the current treatments

The following chromophores and environment/solvent molecules were studied: (i) the female natural hormone estradiol, which is a luminescent hormone due to the presence of the phenol ring with a rich π-system [101–104]; (ii) benzene molecule, which is the origin of many substituted derivatives and which provides a very low absorption probability for the first electronic excited state [105–109]; (iii) 9-cyanoanthracene, which is a molecule with intense fluorescence whose spectral maximum shifts under high pressures [11]; (iv) argon, hexane, cyclohexane, ethanol, and DMSO, used as solvents in experimental investigations of the spectral-luminescent molecular properties.

A canonical NVT ensemble implemented in Tinker [110] treats a molecule of estradiol or benzene solvated by 56 surrounding molecules of ethanol, DMSO, hexane, or cyclohexane for MD modeling.

The number of the molecules is restricted by the boundary conditions of the unit cell with lattice lengths of 24 Å. The solvent density is slightly variable and dependent on temperature and very weakly on the type of solutes (benzene 0.30 g/cm^3 and 0.53 g/cm^3 at 30 and 300 K; estradiol 0.31 and 0.55 at the same temperatures, respectively). The "normal condition" is assumed to be atmospheric pressure (1 Bar) and room temperature (300 K). Each equilibration simulation was performed for 0.5 ns with time step of 1.0 femtosecond (500,000 steps).

Coupling between cyanoanthracene and argon particles was simulated using the MD DL_POLY package [111]. Noose-Hover canonical (NPT) ensembles for high pressure between 1 and 60 kBars and microcanonical (NVE) ensembles for dilute gas with periodical cubic boundary conditions were used. About 1,000 particles were involved in MD run with a time-step of 0.015 ps and total time interval up to 250 ps. The initial number of argons was 1,000, but several of them were replaced by the solute molecule. The "frequency resolution" was accepted as $\Delta\lambda = 4.365$ nm except in the 30 K case where $\Delta\lambda$ was 1.2 nm.

Preliminary relaxations were performed with rigid and fixed solute molecules for all cases. All molecules were completely flexible according to the classical force-field potentials. Tinker MD software with the standard MM3 [110, 112] and MD DL_POLY with AMBER [113, 114] force field parameterizations (VdW nonbonded, bond-length, bending and torsion) were applied except for the bond stretching and angle bending parameters on the phenyl rings. The ideal bond length of carbon hexagonal ring was taken as 1.40 Å on estradiol and cyanoanthracene and 1.38 Å for benzene, ideal angle was 120°. Single nonring carbon–carbon (C–C) and carbon–nitrogen (C≡N) bonds were chosen as 1.42 and 1.16 Å, respectively. These parameters were changed a little for the fluorescent state according to the evaluative formula [9] $\Delta R_{AB} \approx -0.46\ \Delta P_{AB}$, where ΔR is the change of the interatomic distance and ΔP is the change of the bond population (order) at the transition from one state to another. The geometry of the molecule remained close to planar.

After the MD run, the excited states and oscillator strengths of 5,000 conformers of a fluctuating solute molecule were calculated by INDO/sp and CIS implemented in a developmental version of the GAMESS package to construct the statistical spectra [6, 10]. CI matrices are constructed using 10 occupied and 12 vacant MOs (10 × 12) for benzene and estradiol, but cyanoanthracene having a larger chromophore center required a matrix of size (17 × 15). Additionally, the rate constants for radiation decay and the cross sections for conversions were defined for fluorescence. All spectral intensities were normalized to unity except for the benzene sample whose experimental maximum and the most intensive (at 300 K) mode in the spectrum were normalized, while the rest of the spectral bands were rescaled to the intensity of this band with the normalization multiplier. Once calculated, the charge distribution for the atoms (atomic partial charges) for the starting equilibrium structure was invariable during whole MD simulation; consequently, the charge fluctuation is not considered. Several single-point energy calculations of equilibrium structures were performed by

Gaussian, GAMESS, and ADF in different theoretical levels of HF and DFT to show the reason why INDO/sp has been chosen to apply together with the SQMMD method.

3 Results and discussion

3.1 Single-point calculations

In order to choose a method to calculate energies and transition intensities between the ground and lowest singlet excited states, numerous single-point energy calculations have been carried out in various quantum–mechanical theoretical levels implemented in the different standard packages GAMESS [6, 23], Gaussian [17], and ADF [19] (Table 1). One can see that INDO/sp with CIS implemented in a developmental version of the GAMESS [6] provides the best agreement with experimental results that is a consequence of the fact that the specific spectroscopic parameterization has been fitted to reproduce the experimental spectra of the benzene ring and other aromatic conjugated polycyclic and heterocyclic hydrocarbons. This is the rational we had in using this method to calculate the transitions to FC states. Since benzol is the chromophore center of estradiol, and cyanoanthracene is a substituted anthracene the choice of this method seems to be not only rational, but optimal for our specific purposes. Moreover, the calculation only take a few seconds, which is very important for the large number of calculations required for the thousands conformers/structures we have extracted from our MD simulations.

The other semi-empirical method ZINDO [17, 98] gave worse, but satisfactory agreement for benzene and estradiol but failed for cyanoanthracene. The other methods used to calculate the transition energies and oscillator strengths took longer and gave worse results in general (see Table 1). The first excited-state transition energy for benzene is underestimated by all the RHF-CI and TD-DFT methods, while the first excited transition energy for cyanoanthracene is underestimated the RHF-CI method with all of the basis sets. It is dramatically overestimated by the TDDFT method by up to 100 nm. The first excited-state transition energies for estradiol calculated by TDDFT, except for the TDDFT-lsda,lanl2mb and TDDFT-lsda,3-21 + ** methods, are reasonably accurate, but the values calculated for all the RHF-CI methods are strongly underestimated.

Among the other methods used, the results for all three molecules with the hybrid B3LYP exchange correlation

Table 1 Single-point energy calculations of the lowest singlet states obtained in the different levels of quantum–mechanical theories using the various basis sets and exchange correlation functionals for DFT methods

	Benzene	Cyanoanthracene	Estradiol
Experiment	254.8	382.1	290.0
INDO/sp&CIS (GAMESS)	**250.7**	**378.9 (0.34)**	**288.6 (0.06)**
In GAMESS			
RHF-CI, 6-311	230.4	337.5 (0.30)	209.7 (0.08)
RHF-CI, tzv	230.4	339.1 (0.30)	212.3 (0.08)
TDDFT-blyp, nd-diff	**239.3**	488.7 (0.06)	297.5 (0.001)
TDDFT-blyp, np3-diff	232.0	476.0(0.07)	293.7 (0.001)
TDDFT-svwn, 6-311	231.3	475.5 (0.07)	**275.6 (0.04)**
RHF-CC, CR-EOM, 6-311	236.6	Mem required 430 MW	Mem required 950 MW
In GAUSSIAN			
ZINDO	**264.5**	445.0 (0.31)	**292.4 (0.04)**
RHF-CI, 3-21	190.7	329.2 (0.30)	203.1 (0.08)
RHF-CI, 3-21 + **	198.4	**338.3 (0.30)**	212.4 (0.08)
RHF-CI, 6-31	194.2	334.0 (0.30)	206.0 (0.07)
RHF-CI, 6-311	196.7	337.5 (0.30)	209.7(0.08)
TDDFT-lsda,3-21 + **	203.6	**375.8 (0.21)**	220.0 (0.07)
TDDFT-lsda,lanl2dz	232.3	474.7 (0.07)	273.3 (0.04)
TDDFT-lsda,lanl2mb	201.9	404.6 (0.08)	340.1(0.00)
TDDFT-b3lyp,3-21	218.7	428.0 (0.09)	248.7 (0.04)
TDDFT-b3lyp, dgdzvp	230.2	455.2 (0.08)	260.2 (0.05)
TDDFT-rbvp86,dgdzvp	**236.9**	493.8 (0.06)	**276.7 (0.04)**
TDDFT-rb3pw91,dgdzvp	228.5	452.6 (0.08)	258.9 (0.05)
In ADF			
VWN, Becke–Perdew, DZ	229.4	472.2 (0.07)	267.2 (0.03)
VWN, Becke–Perdew, TZ2P	**238.2**	494.0 (0.06)	**279.8 (0.04)**

First column contains methods to obtain results, the rest of them provide energy E of excited state S_1 in (nm) and oscillator strength f (unitless), excepting benzene where $f = 0.00$

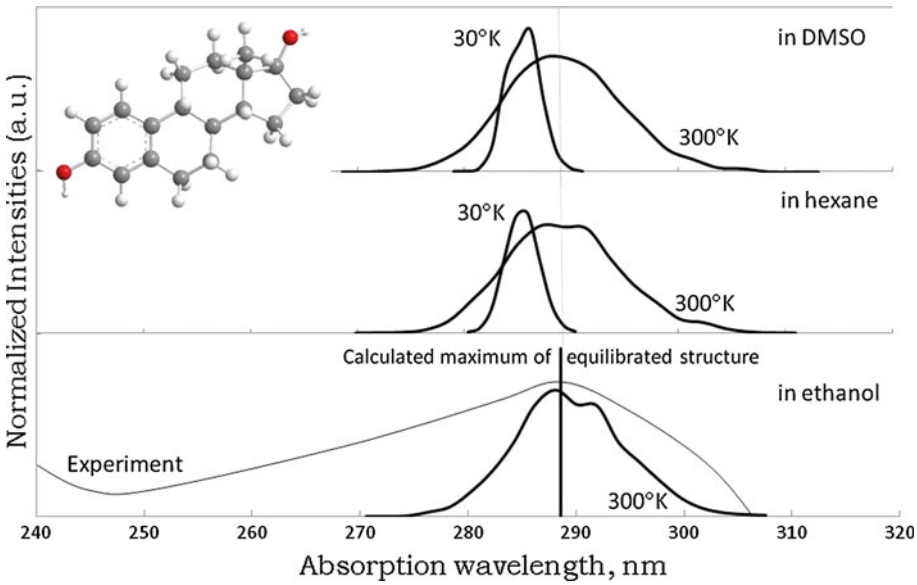

Fig. 2 Estradiol. Empirical absorption spectrum in alcohol at 20 °C [27], statistical profiles in ethanol at 300 K, and the lowest electronic state in equilibrium position denoted by the *straight vertical line* (*lowest rectangle*); spectra of the molecule in DMSO at 300 K and narrow one at 30 K (the *middle picture*); as well as spectra in hexane at 300 and 30 K. The stereo-chemical structure is given in the *upper-left corner*

functional and the 3-21 or better dgdzvp basis set are very far from the experimentally measured values. It has been previously documented that this hybrid exchange correlation functional drastically underestimates the transition energies for states involving charge transfer. The CAM-B3LYP and CAM-B3PW91 hybrid exchange correlation functional has been specifically developed to correct this problem with the B3LYP hybrid exchange correlation functional [65]. The most appropriate results of each theoretical level are marked by the bold font in Table 1. The GAMESS, Gaussian, and ADF programs all use the Davidson iterations algorithm to find CI eigenvalues and eigenvectors. It should be noted that the same basis set and exchange correlation functional in the case of DFT provide inconsistent deviations from the experimental data for molecules containing π-conjugated systems. This could be due again to the problems with the states involving charge transfer. Here, one should use a method that does not give very different errors for different excited states, since the ordering of the states is very important. The methods of choice by many for the calculation of electronic excited-state energies and electric dipole transitions moments are the CAS-PT2, CAS-PT3, and CAS-DFT methods developed in the group of the late Bjørn Roos in Lund [26, 34]. But these methods are certainly not black box methods, like the TD-DFT methods with appropriately chosen XC functionals, the method of choice most recently being the CAM-B3PW91 method implemented now in Dalton and Gaussian 09 [65].

3.2 Estradiol

The calculated transition energy for a transition from the ground singlet state to the lowest excited singlet state of the molecule frozen in its equilibrium configuration coincided pretty well with the experimental maximum (Fig. 2). Calculations with other theoretical methods did not provide such good results, as shown earlier (Table 1). The estradiol structure was optimized at the MM2 and MOPAC-AM1 levels of theory as implemented in the ChemOffice software. However, the $\pi \rightarrow \pi^*$ transition within the benzene ring is responsible for this electronic transition. A planar ring structure resulted, which satisfies the customary conditions required for a flat, planar benzene ring. The bond lengths were found to be 1.40 Å and valence angles within the ring were found to be 120°, consistent with sp^2 hybridized orbitals. A more accurate geometry for the remaining part of the molecule is not needed because its influence on the excited electronic state composed mostly by the filled π-electron orbitals of the benzene ring is negligible [104]. The INDO/sp calculations at the equilibrium structure gave information about the excited states. The electronic energy levels define the position of the spectral maxima and the calculated oscillator strength gives an estimate of the absorption intensity.

The spectra of estradiol dissolved in ethanol, DMSO, and hexane at 30 K and 300 K (Fig. 2) have almost the same line widths in different solutions, but they are narrower at the lowest temperature. It is obvious that molecular oscillations are smaller in a colder system that is responsible for the weaker (less intense) spectrum at lower temperatures. The band maxima are shifted to the shorter-wavelength UV region relative to the energy calculated and observed in its equilibrium ground state geometry. At lower temperatures, the simulations describe the peaks in the experimental absorption spectra more precisely. The experimental spectrum in ethanol at 20 °C is a smooth curve without a vibrational structure (a vibrational manifold is not observed). The spectral shapes obtained with a

frequency resolution of 1.2 nm in the cold systems and 2.0 nm in the higher temperature systems are different and depend on the surrounding molecules, and possibly also on a different distribution of conformers which are populated. These differences in the spectral shapes can be explained by our simple approach and no systematic dependencies needed to be defined. It should be noted that the profiles are strongly determined by the MD force-field parameterization. Minimally increasing the ideal bond lengths of the benzene ring C–C bonds leads to a displacement into the longer-wavelength part of spectrum and, vice versa, decreasing of the ideal bond lengths of the benzene ring C–C bonds leads to a displacement into the shorter-wavelength part of the spectrum. Parameters for molecules and environment for use with the SQMMD method should be developed in the future to allow one to more accurately reproduce the spectra and make the simulations closer to realistic experimental conditions. Nevertheless, the experimental spectrum was reproduced by the statistical curves with satisfactory agreement, taking into account that the experimental spectrum is measured under more elaborate environmental conditions. As such, the solute molecules experience more intricate interactions with the environment and other molecules, as well as experience the effects of other vibrational modes, both ground and other higher excited vibrational and electronic states, effects not taken into account in our current model. The theoretical spectra were obtained using only the lowest excited electronic state. Moreover, our calculations were carried out in the framework of the frozen orbital approximation using INDO/sp and CIS methods where transitions proceed to the most probable FC states of each conformer but less possible transitions to other vibrational sublevels are omitted. This leads to a narrowing of spectral line widths, which of course must be taken into account, especially at higher temperatures where the broadening is observed. Comparing with our previous work [6], this affect is not so evident for the broad absorption spectra when one uses numerous excited states because the maxima have been defined in the correct position. Here, the vibrational broadenings overlap with each other to form a broadened (broader) peak. The question is which mechanism, or combination of mechanisms is the more accurate and physical model. In one case, one models the broadening to a large number of perturbed excited electronic states, while in the other case, one calculates the FC vibrational overlap integrals for a smaller number of perturbed excited electronic states, each of which need to be optimized, the Hessians calculated, and the complete set of vibrational overlap integrals calculated.

3.3 Benzene

The oscillator strength for a transition from the ground electronic singlet state to the first excited singlet electronic state at the equilibrium ground electronic-state geometry is negligible, that is, its oscillator strength is either zero or close to zero. This criterion (selection rule) makes the absorption transition, $S_0 \rightarrow S_1$, forbidden. However, in the experimental spectra, one observes a weak band, which has been assigned to an excitation due to the $S_0 \rightarrow S_1$ transition. The experimental absorption spectrum in cyclohexane at 23 °C is presented in Fig. 3 [109]. The molar absorption coefficient is 210 $M^{-1}cm^{-1}$, with the maximum at 255 nm. The symmetry-forbidden electronic transition between these states is permitted in nonequilibrium structures, that is, when the benzene ring is no longer strictly planar. Theoretical spectra with nonvanishing intensities are constructed using the MD statistical technique (Fig. 3). The intensity increases together with an increase in the temperature. The calculated excitation to the first excited electronic state, S_1, is predicted to occur at 250.7 nm for benzene in its equilibrium ground state geometry with zero intensity (the oscillator strength is predicted to be zero). As one can see, this is the best approach to the experimental

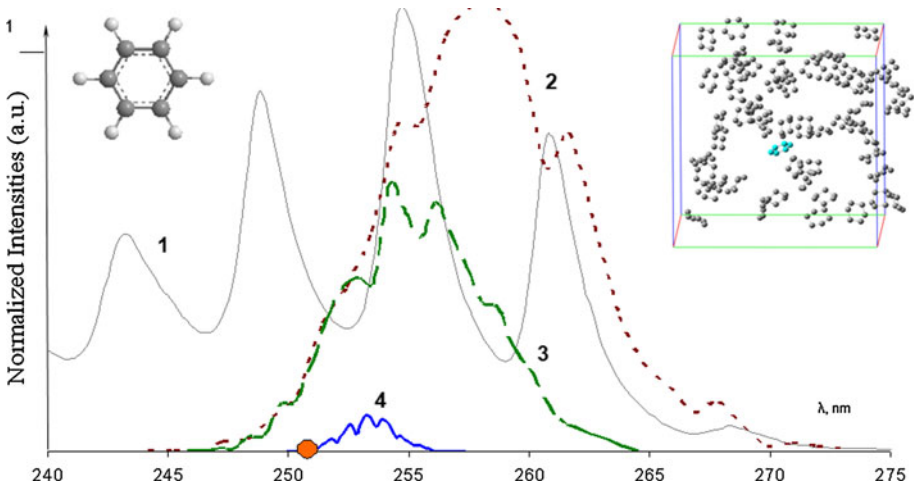

Fig. 3 Benzene absorption spectra. Experimental curve at 23 °C in cyclohexane (*solid*, **1**) [32]. Statistical graphs at $T = 300$ K (*dotted*, **2**), $T = 150$ K (*dashed*, **3**), and $T = 30$ K (*solid smallest*, **4**) in cyclohexane. The first electronic state at 250.7 nm of equilibrium structure with zero oscillator strength (*circle*)

data (Table 1). But for the conformers observed from our MD simulations in cyclohexane solution at 30, 150, and 300 K, the calculated oscillator strengths range from zero to maximal values of 0.0008, 0.0086, and 0.0190, respectively. These values being the corresponding spectral heights and integrated areas under the curves (total intensities). The respective frequency resolutions of 0.266, 0.643, and 2.129 nm were defined if spectral widths are divided into 29 partitions. This number was chosen to keep the frequency resolutions near 2 nm in the system at $T = 300$ K. The spectrum expands into the long-wavelength region starting from the point of zero intensity corresponding to a transition of the isolated molecule in its equilibrium structure (Fig. 3). The statistical spectra are smoother and narrower than the experimental spectra, though five maxima can be recognized. Four intense peaks and weak maximum at the end of long-wavelength wing define the spectral profiles. Some possible reasons for the disagreement between the theoretical and experimental spectra are due to perhaps the aforementioned problems pertaining to the choice of force-field parameters, environmental influences not taken into account as well as the energies of electronic transitions being calculated using the methods described above.

3.4 Cyanoanthracene

The idea to use cyanoanthracene has been motivated by the experimental research devoted to studying the influence of different pressures on the lifetime of the fluorescence state(s) of both 4-(10-cyano-9-anthracenylmethyl)-*N*,*N*-dimethylaniline (CADMA) and the simpler structure 9-cyanoanthracene (9CNA or CADM, Fig. 4), and these molecules embedded in a polymethylmethacrylate (PMMA) film [11]. The fluorescence spectra of these two molecules are very similar and their photophysical CADM properties in general define CADMA's optical characteristics.

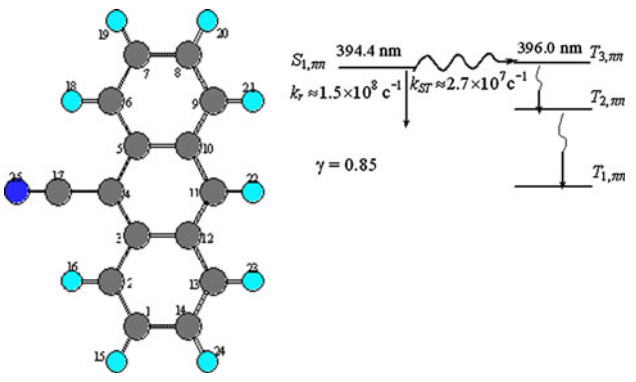

Fig. 4 The stereo-chemical structure and photophysical scheme of CADM that includes singlet S and triplet T energy levels, the rate constants of radiation k_r and cross-section k_{ST} transitions, as well as fluorescent quantum yield

Single-point quantum-chemical calculation Before investigating the oscillations of the molecule under TD conditions, the structure and properties of the isolated rigid CADM molecule should be studied. This molecule belongs to the anthracene class with well-known spectral-luminescence properties and can be considered as a cyano-substituted anthracene. Its photophysical processes and energy scheme should be close to those of anthracene, while the C≡N cyano-group produces a perturbation.

The unexcited ground electronic state structure of the benzene ring was assumed to correspond to the commonly used structure of aromatic carbon cyclic compounds, in which all C–C bond lengths are 1.4 Å and valence angles are equal to 120°. The single nonring carbon–carbon (C–C) and carbon–nitrogen (C≡N) bonds were chosen to be 1.42 and 1.16 Å, respectively. The calculated transition energy/absorption frequency for the first electronic absorption band maximum was in the red spectral region, with $\nu(S_{0,0} \rightarrow S_{1,n})$ being 26,392 cm^{-1} (378.9 nm) and having a large oscillator strength f_x of 0.34. Various experimental investigations have located the maxima for the first electronic absorption band at 26,170 cm^{-1} (382.1 nm) [115].

In order to calculate the fluorescence maximum, the molecular geometries were determined for the excited electronic states according to the methods described in Methodology and computational details section [9]. Molecules in the first excited singlet state S_1, which has a calculated transition wavelength of 394.4 nm, return to the ground electronic singlet state by photophysical processes proceeding in the molecule that can be detected by emission of light (fluorescence), which has been confirmed by the measurable experimentally determined quantum yield for fluorescence (Fig. 5). The quantum yield for fluorescence, $\gamma = 0.85$, was estimated according to the vertical Jablonski diagram presented in right portion of Fig. 4, where S and T correspond to singlet and triplet states, respectively, and are marked with numbers and types of transition between molecular orbitals, all of which have π symmetry. Some portion of the excited electronic energy decays through the cross-section channel due to a spin-orbital coupling mechanism connecting the $S_{1,\pi\pi}$ and $T_{3,\pi\pi}$ state with a probability for singlet–triplet conversion, k_{ST}, of $\approx 2.7 \times 10^7$ compared with the fluorescence probability, k_r, of $\approx 1.5 \times 10^8$. The experimental efficiency for fluorescence is about 90% [115]. The calculated spectral properties of the individual molecules are most similar to those in the fluorescence excitation spectrum for the structure found in argon at a pressure of 210 Torr [116]. The CADM fluorescence lifetime τ_f in the gas phase was short ($\tau_f \approx 3$ ns) compared with lifetime in solution ($\tau_f \approx$ 14–15 ns). The band origin, $\nu(S_{0,0} \rightarrow S_{1,n})$, of the

observed vibronic manifold was found to be at 382.1 nm (26,173 cm^{-1}).

If molecules are flexible then their high symmetry can be broken via external collisions and in the "out-of-plane" case, the distortions of the molecular planar structure lead to mixing of the π- and σ-orbitals, which is not possible for the strictly planar structure. In addition to deviations from planarity due to the collisions, there is an increase in the spin-orbital interaction, which consequently and subsequently leads to quenching of the fluorescence. This effect, among others, can be investigated via an MD simulation which includes the effects in the TD perturbation applied to the system. Here by varying the perturbation, one can see the effects of each, and also possibly combinations of perturbations, when one or more are applied at the same time, or together, but with time delays between their applications.

MD and QM simulation of the oscillating molecules To date there has been no reported experimental absorption spectra reported at high pressure (and hence pressure dependence), and our here reported pressure dependence of the absorption spectra is hence more predictive than comparative in nature; except for the spectral results reported for weak TD perturbational conditions which can be compared to the experimentally observed spectra. The initial MD system was at low temperature ($T = 30$ K) and pressure ($P \approx 0.4$ bar). Two absorbing systems, both at a temperature of 300 K and each at significantly different pressures (the first one at almost normal pressure, 4 Bar, and the second one at a very high pressure, 20 kBar) were studied (Fig. 5). The straight green dotted line corresponds to the calculated electronic absorption spectrum for the first excited electronic state of the flat rigid molecule. Spectral peaks of the molecule in dilute gas under low temperature can be seen to be pretty close to the wavelength of the flat rigid structure. The increase in the temperature is the main reason for the visible shift up to 5 nm of the absorption maxima, spectral broadening, and maxima losing intensities. The spectral broadening is from 22 nm at $T = 30$ K to 80 nm at $T = 300$ K. The two spectra simulated at different pressures, 4 and 20 kBars, respectively, but at constant temperature of 300 K almost coincide, which seems to indicate an insensitivity to changes in the pressure. The CADM simulations undertaken at various pressures produce spectra with similar intensities and different shapes, while the temperature of the simulations defines the spectral widths. The spectrum of CADM generated from the MD simulation run at 4 Bar is smoother than the one generated from the MD simulations run at 20 kBar, perhaps due to the fact that at a lower pressure more internal degrees of freedom in the gas phase are accessible (a larger phase space is sampled). At high pressure the vibrations of molecules "dissolved" in the solution and modeled by the NPT ensemble appear to be affected by the higher concentration (per volume, but of course not number of molecules which has not changed) because of the smaller nonconservative volume. At higher pressure, the density decreases and one can observe changes of state, gas to liquid and finally liquid to solid. In our systems, we have chosen to run NPT MD simulations, so we are able to observe volume and density changes, and the effects these macroscopic effects have on the structural and spectroscopic properties of the individual molecules.

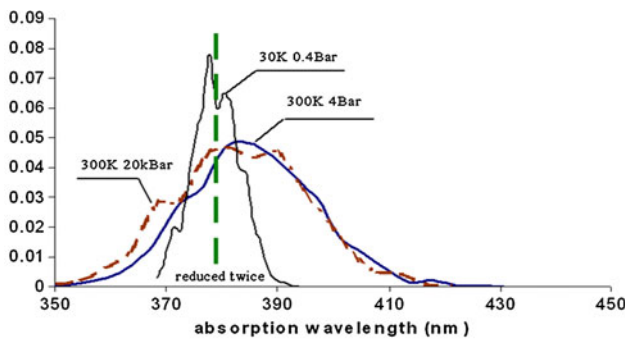

Fig. 5 The theoretically reconstructed absorption spectral bands (intensity in relative unit) of cyanoanthracene under different TD condition (temperature in K, pressure in *Bar*) in argon solvent

Compared with the absorption spectra, it can be noted that the peaks in the fluorescence spectra are shifted to the longer wavelength due to shifts in the energy levels of the first electronic singlet levels for the flat frozen absorption geometry and the molecular structures in the excited electronic state (Fig. 6). Profiles of absorption and fluorescence spectra at $T = 30$ K have mirror symmetrical vibronic (AQV) profiles. Two large maxima are observed in both the absorption and fluorescence spectra. The spectra have the typical shape for the molecule based on the anthracene chromophore fragment, but these maxima cannot be assigned with certainty for all the vibrational modes because a technique for deconvoluting such kinds of spectra constructed by the SQMMD method is still being developed. Note that the relative intensities of the bands are also different. These fine features for both the absorption and fluorescence spectra have a wealth of information, which can now be partially interpreted within our model. But for the interpretations to be meaningful, they must mimic what is actually observed in the experimentally observed absorption and fluorescence spectra, and the changes which occur as a function of solvent polarity, temperate and pressure, and then the combination of one or more of these perturbations.

Increasing the temperature makes the spectra wider in one wavelength interval (again approximately from 20 nm at $T = 30$ K to 80 nm under $T = 300$ K) for all pressures (Fig. 7). When the pressure was changed, the vibronic (AQV) profiles also changed. At room temperature in the

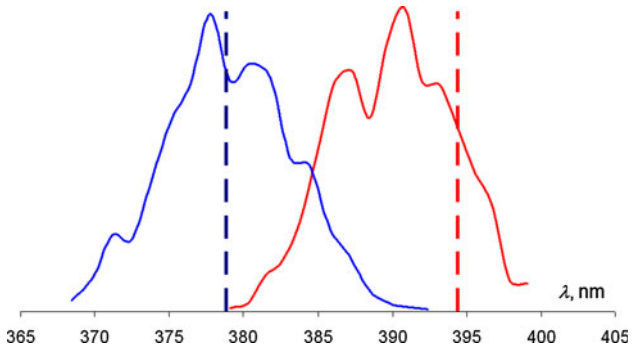

Fig. 6 Both theoretical absorption (*left*) and fluorescence (*right*) bands under weak TD condition ($T = 30$ K and $P = 0.4$ Bar) using a frequency resolution equal to 1.2 nm. The intensities are scaled to the main maximum. The *straight lines* correspond to absorption and fluorescence states of the molecule in equilibrium positions

normal condition, the fluorescence spectral shape becomes less sharp and washes out with applied pressure, as one changes from 1 to 20 kBars. At 40 kBars, a distinct structure comes back which is again lost at 60 kBars. This phenomenon can be explained as an attempt to join the liquid and solid phase conditions of solvent and spectral properties. The NPT ensembles, which conserve both the pressure and temperature, allow the concentration in volume (density) to be varied which can lead to a phase change. The volume and hence density changes, and this can be used as an order parameter to monitor the phase change. The solvent remains liquid at 20 kBars and become solid above this pressure. The molecule is more flexible in the fluid state and has more degrees of freedom than in the solid. At a pressure of 40 kBars the system can be in the "transitional phase" and the system has mixed properties, while at 60 kBars the system becomes completely solid because fluctuations are decreased due to restricted motions. This is only a supposition or an assertion and NOT a certainty. It seems to be plausible based on the support this idea has based on comparing the experimental and calculated spectral data. One can see that the calculated (under 40 kBars, Fig. 7) and experimental (under 2.60 GPa = 26 kBars, Fig. 8) spectra look similar [11]. Probably, at the pressure of 40 kBars, there is a kind of phase transition for the argon solvent, whereas for the PMMA films, a pressure of 26 kBars is required for the similar condition (effect to occur). It would be interesting to simulate the two solvent systems as a function of temperature and pressure alone, and see what features are due to the solvents and which are due to the solute molecule. It would also be interesting to perform simulations on the isolated molecule and in the solid and liquid states. But many molecules decompose before the solid actually melts, so one must be careful with classical MD simulations, where one can heat a system to a temperature where the real compound starts to decompose, break down. Hence, it

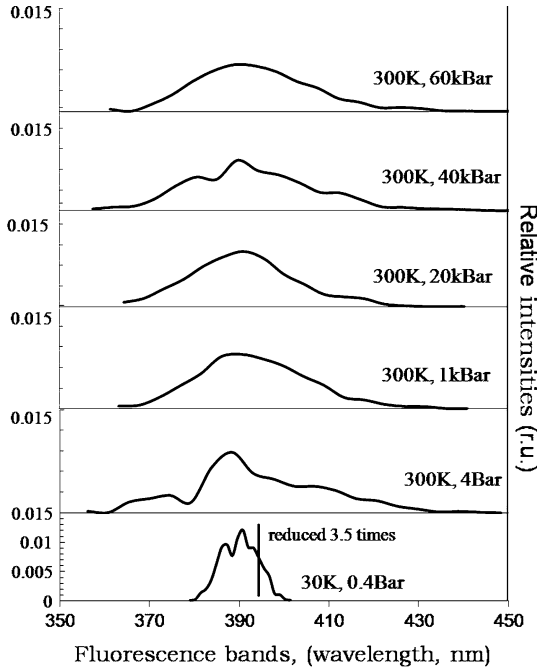

Fig. 7 The theoretically reconstructed fluorescence spectral bands of cyanoanthracene under different TD condition (temperature in K, pressure in Bar) in argon solvent

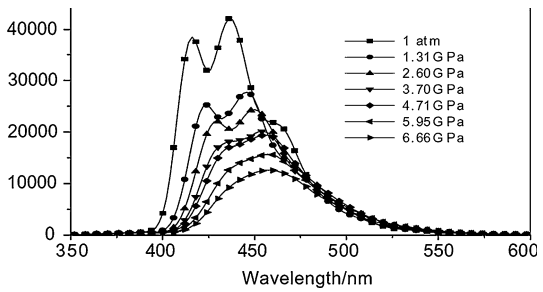

Fig. 8 The experimental pressure-dependent fluorescence spectra (intensity in a.u.) of cyanoanthracene in PMMA was reported in [9]

is much better to perform ab initio wave function theory or DFT Born–Oppenheimer MD simulations, where such processes can, should, and do occur. Of course, they (DFT-BOMD simulations) are much more expensive than the corresponding classical molecular mechanics force field MD simulations. In our work here, we have used the classical molecular mechanics force field MD simulations to get the first-order effect that temperature and pressure have on the structure of our solutes and their environment. Chemical effects are not treated with this model. Such effects will be considered in a future work.

The rate of radiation that reflects the probability of this process is maintained between 10^7 and 1.5×10^8 s^{-1} throughout the entire MD run. Each local γ was calculated according to the probabilities k_r and k_{ST} for a current conformer whose triplet state was chosen as similar as

possible to the type of $T_{3,\pi\pi}$ in the equilibrium structure. Each magnitude of quantum yield was averaged over the corresponding wavelength interval $\Delta\lambda_k$ and multiplied by $p_{\Delta\lambda}$ and averaged k_r. The relative radiation intensities were integrated to a fluorescence curve. Emission spectral contours differ from the ordinary distribution $p_{\Delta\lambda}$ because the fluorescence quantum yields γ for different fluctuating structures undergo substantial dispersion between 0.00 and 0.96.

Neither valence angles nor dihedrals reach the magnitudes when the molecular structure is changed catastrophically and can be assumed as another molecule with different photo-physical properties. There is no significant change in these angles, probably because the molecule undergoes a uniform influence from argon solvent under different TD condition and therefore there is no big wavelength shift. Probably, if the solvent is more complicated than argon and its influence is inhomogeneous, it will be possible to obtain a stronger dependence of CCN angle on TD condition.

CADM embedded in an argon solvent treats the effects due to the homogeneous TD influences and there is no reason to expect large structural changes. The spectral shifts can also be obtained for much more complicated compounds and solvents (complex CADM-PMMA, for instance) under anisotropic pressure influence to obtain more similar spectra to the experimental results. Perhaps, the simple solute–solvent system is most reasonable explanation for the obtained disagreement. The problems have been discussed in the sections on the estradiol and benzene cases.

3.4.1 *Solvent influence*

This extra-section is devoted to the effects that the solvent molecules can and do have on the excitation of solute molecules in the ground electronic state into the lowest electronic excited states, and subsequent emission back to the ground electronic state, the spectra of which we are attempting to and have simulated and are the topic of our discussion. Obviously the coupling of a molecule to and with its environment leads to distortion/change of the molecular structure due to electrostatic, VdW and other forces. These geometrical deviations certainly induce changes in the electron cloud (orbitals) that provides perturbations in both MOs and shifts in the excitation energies. The much more complicated matter is whether the electronic orbitals of the solvent molecules significantly contribute energy directly to excite a solute molecule along with changes in the MOs of the solute molecule. It is well known, for example, from experimental data and numerous theoretical works that the electronic cloud of water perturbs the MOs of solute molecules and, therefore, the excited electronic states of organic molecules in aqueous solution. But there is unfortunately much less theoretical work devoted to this and other related systems, particularly neutral aprotic and nonpolar solutions, for which there is a wealth of experimental data waiting to be interpreted by high and medium level molecular simulations. It is very important to have such information/data for testing the efficiency and accuracy of QM solvent treatments, for determining whether one should and can neglect nearest neighbor solvent molecules, or whether they must be included when one calculates the electronic energies of the solute, and subsequently various molecular properties, including electronic excited state absorption, followed by subsequent emission back to the ground electronic state. In many cases, there is energy and momentum transfer not only between the solute and the solvent molecules, but also between various parts (chromophores) of a large biomolecule. For example, there is both electron and energy transfer within the photolyase class of proteins after absorption of a blue photon in the presence of damaged DNA [16]. The absorption of the blue photon is necessary for the photolyase protein to repair the damaged DNA molecules which are bound to the photolyase proteins by nonbonded interactions, and are released back into the environment after repair. Clearly to understand such processes at a molecular level will require more work, and such problems are motivation for the work which we are undertaking here.

As a first step to such complex problems, all QM calculations in this work were carried out for isolated solute molecules (in the absence of the complex biological environment) of estradiol, benzene, and cyanoanthracene. This approach is taken in order to completely document our approach for a set of representative examples. The effects due to the complex biological environments will be considered in future works.

Estradiol is included because its chromophore is a benzol ring. In addition, the benzene group with a small number of attached alkyl groups is conceptually easy to study. Furthermore, it is of more interest and fruitful to consider examples where solute–solvent couplings are expected to be much stronger due to the comparatively similar structures of benzene and cyclohexane (Fig. 9a) or CADM under severe TD conditions, with a $T = 300$ K and a $P = 20$ kBars (Fig. 9b). Complexes of conformers surrounded by 6 molecules of cyclohexane for the benzene case and 36 argons near CADM were taken during the last steps of MD simulations. Since comparative analysis is required and it is not needed to obtain energies of high accuracy, QM calculations were carried out by the Gaussian software at the TD-DFT level using the split valence 3–21G basis set and B3LYP hybrid exchange–correlation functional for both molecules in their surroundings.

If one assumes the following notation where the MOs are counted starting from the highest occupied molecular

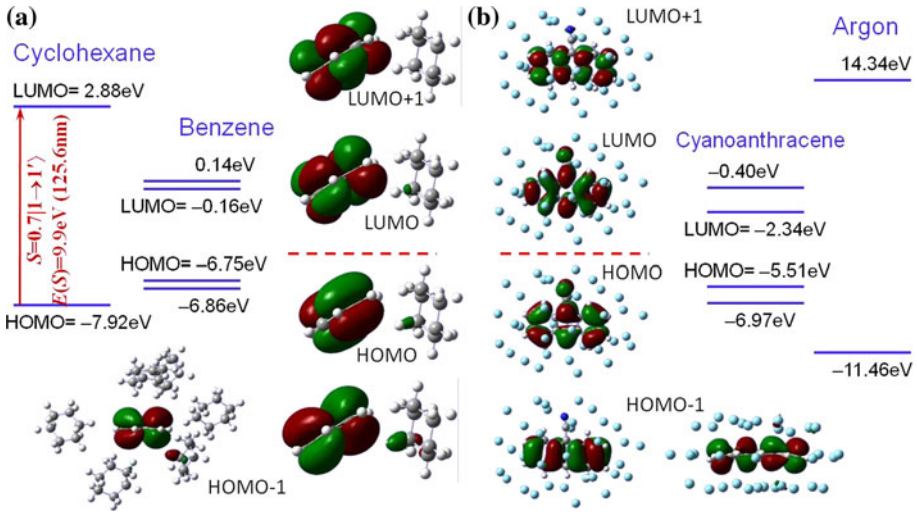

Fig. 9 MOs localized over AOs of benzene dissolved in cyclohexane (**a**) and cyanoanthracene surrounded by Argon atoms (**b**)

orbital (HOMO) in one direction and from the lowest unoccupied MO (LUMO) to the inverse direction then HOMO–1 $\equiv|2\rangle$, HOMO $\equiv|1\rangle$ and LUMO $\equiv|1'\rangle$, LUMO+1 $\equiv|2'\rangle$, LUMO+2 $\equiv|3'\rangle$. In the CIS case $S_i = \sum_{lk'} A_{i,lk'}|l \to k'\rangle$ and energies of first excited state for conformations such as benzene + 6 cyclohexanes, benzene + 1cyclohexane and bare benzene, respectively are:

$$S_1 = 0.47|2 \to 1'\rangle + 0.20|2 \to 2'\rangle - 0.24|1 \to 1'\rangle + 0.44|1 \to 2'\rangle; E(S_1) = 224.2 \text{ nm} \quad (f = 0.002)$$

$$S_1 = 0.48|2 \to 1'\rangle + 0.17|2 \to 2'\rangle - 0.21|1 \to 1'\rangle + 0.46|1 \to 2'\rangle; E(S_1) = 223.7 \text{ nm} \quad (f = 0.001)$$

$$S_1 = 0.46|2 \to 1'\rangle + 0.22|2 \to 2'\rangle - 0.27|1 \to 1'\rangle + 0.44|1 \to 2'\rangle; E(S_1) = 222.9 \text{ nm} \quad (f = 0.001)$$

It should be noted that second excited states for the same structures are $E(S_2) = 194.7$ nm $(f = 0.019)$; $E(S_2) = 194.2$ nm $(f = 0.028)$; $E(S_2) = 192.8$ nm $(f = 0.014)$, respectively, where f is oscillator strengths. Errors are less than 1 percent (0.58% for S_1 and 0.98% for S_2). Closer to the first energy excitation of cyclohexane (125.6 nm or 9.87 eV), higher electronic states of benzene should be perturbed by an admixture of MOs localized on solvent molecules with those of benzene. It needs to be noted that HOMOs of benzene and cyclohexane are much closer to each other than their LUMOs, which leads to a slight admixture of AOs of a cyclohexane molecule to the occupied MOs of benzene. The weak delocalization explains the small shift of the excitation levels. The weak interactions between benzene and the nearest neighbor cyclohexanes are depictured in Fig. 9a for all four important MOs responsible for forming the lowest energy excitations. Both the highest occupied molecular orbital (HOMO) and lowest unoccupied molecular orbital (LUMO) include visible contributions from AOs localized on part of the cyclohexane, though this participation was considered to be very weak. Analysis of the excited energies and of the configuration expansion obtained for all three conformations shows that the other solvent molecules included in the closest (nearest) solvent shell make much smaller contributions to the excitation energies that can not be seen in Fig. 9a.

One can hypothesize and criticize that this single conformation of the droplet is not chosen appropriately to demonstrate the influence of the solvent on excitation energies for the solute. There is a reasonable way to increase the perturbation strength, which is to decrease the separation between the solute molecule and the solvent molecule to its minimal value that is determined by VdW forces and distances between the carbon and hydrogen atoms. The major interatomic nonbonded VdW potential function for the MM3 force field parameterization [112] is assumed to have the form $E_{\text{vdw}} = \varepsilon_{ij}[184000\exp(-12.0d_{ij}/D_{ij})-2.25(D_{ij}/d_{ij})^6]$, where ε_{ij} is an energy scale factor for each atom pair which measures the interaction energy, d_{ij} is the effective distance between interacting centers of two atoms, and the separations D_{ij} represent the VdW's radii of the atoms as $D_{ij} = D_i + D_j$. The following values of D_i radii were taken for: aromatic saturated carbons in benzene ring $D_i(\text{C}_\text{B}) = 2.04$ Å; aliphatic carbons $D_i(\text{C}_\text{A}) = 1.96$ Å, and hydrogens $D_i(\text{H}) = 1.62$ Å that very much restrict (dependent on ε_{ij}) approaching atoms to get closer than separations $D_{ij}(\text{C}_\text{B}\ldots\text{C}_\text{A}) = 4.00$Å, $D_{ij}(\text{C}_\text{B}\ldots\text{H}) = 3.66$ Å or $D_{ij}(\text{H}\ldots\text{H}) = 3.24$ Å, respectively. Thus, we have found that the conformation with minimal distances between benzene and cyclohexanes such that the C…C interatomic distances is equal to 3.6 Å and H…H

interatomic distances equal to 2.1 Å, respectively, that are shorter than the VdW distances and depend on the values of the energy scale factor. Several tenths of ångstroms can't change remarkably the energy of electronic excitation. It should be concluded that in the zeroth order approach for the first two excited states of molecules with the benzol chromophore center dissolved in cyanohexane under normal conditions, it is possible to calculate for the isolated molecule to obtain an appropriate spectrum corresponding to spectra for conditions in the gas and liquid phases. Here, one assumes that there is not a strong interaction between the solute and solvent molecules as found for the alanine dipeptide and the zwitterionic species of L-alanine and L-histidine in aqueous solution [15, 16, 46, 57–59, 89, 90].

The sample of cyanoanthracene in argon solutions at the huge pressure up to 60 kBars seems to be different because VdW distances can be shorter than under the normal condition that in principle could lead to higher perturbation. The 20 kBars is enough high pressure to be far from the normal condition and it seems to be a quite representative case. Firstly, argon AOs can be included into a linear combination to form MOs of a total system and within this paradigm it is possible to say that there should be MOs localized mostly or partially on argon atoms. Such kinds of MOs can be seen (Fig. 9b) very far from the energy levels of the HOMO and LUMO for cyanoanthracene and several other occupied and virtual MOs in CADM, though one can observe a very weak perturbation in HOMO–1 by AOs of the nearest argon atoms. The following 6 electronic excited states have almost the same values for their electronic transitions energies (and oscillators strengths) for both the isolated case and for being dissolved in CADM: their values in nm (unitless for oscillator strengths), 417.2(0.111), 318.5(0.031), 287.2(0.002), 253.6(0.006), 249.6(0.071), 236.5(1.433) for the isolated case versus 412.3(0.108), 315.2(0.024), 282.7(0.002), 251.7(0.003), 247.6(0.043), 232.5(1.425) for being dissolved in CADM, respectively. Errors do not exceed 1%. The expansion over molecular configurations is the same for both cases $S_1 = 0.62|1 \rightarrow 1'\rangle$.

Of course, this perturbation has arisen due to the large pressure that allowed argon particles to concentrate around CADM and approach this molecule to 2.4 Å when VdW distances are defined by the AMBER parameterization set [113, 114] as σ_{ij}(C…Ar) = 3.48 Å and σ_{ij}(H…Ar) = 2.87 Å where the interatomic nonbonded potential is expressed through $U_{ij} = 4\varepsilon_{ij}[(\sigma_{ij}/d_{ij})^{12}–(\sigma_{ij}/d_{ij})^{6}]$.

Thus, one should assume that for the discussed approach, QM calculations of bare aromatic molecules dissolved in the suggested solvents were reasonable, though at least, first solvent shells have to be included to construct more precise spectra.

4 Conclusions

The four main results of this work are:

1. Electronic transitions calculated for conformers obtained from the MD simulation(s) can be "integrated" in such a way to generate a simulated electronic absorption spectra that is associated with a statistical ensemble which results from the MD run.
2. The vibrationally and collisionally perturbed structures allow one to find nonzero transition probabilities that are forbidden for equilibrium planar structure. In the case of the first long-wavelength band in benzene, the larger distortions are responsible for the broader and more intense absorption spectrum.
3. Emission spectra also can be constructed in a similar manner if all photoprocesses consistent with radiative decay are taken into account. In addition, the MD force-field parameters must be adjusted to take into account the changes in their values which occur due to the stereo-chemical structure of the electronically excited state of the molecule being different from that in the ground electronic state. These can be determined by optimizing the structures of the electronically excited state, calculating the Hessian and other molecular properties, and fitting this ab initio and/or DFT and experimental data to the functional form for the potential energy surface, similar to what has been done to generate the second generation molecular mechanics forces fields [117].
4. The vibrational width depends on both the temperature and pressure, and the temperature and pressure broadening define the spectral width and shape that is associated to the specific TD phase. This fact was demonstrated by theoretical statistical mechanical simulation of the electronic spectra: both the electronic absorption and fluorescence spectra.

Force-field bonds stretching, bending and torsion parameters among others should be modified more precisely for photophysical purposes involving temperature and pressure dependencies. We have discussed above how this could be done. Solvent influences and solvatochromic shift can be included in generating the spectral curves, that is, in simulating the experimental spectra, including the line widths. Perhaps, the correlation between computed "time-resolution" and vibrational relaxation time should be discussed and defined more accurately. Some corrections at the expense of, for instance, a "unfrozen orbital or movable nuclear core" approximation in frameworks of various theoretical levels of calculating vibrational modes of ground and excited states and transitions should be taken into account to more realistically simulate the electronic transitions and experimental spectra where all possible (not

only most probable) transitions between different vibrational sublevels will be treated.

In the future, we plan to continue to work on this problem, and moreover, we recognize that one will need to assign vibronic maxima using a DOS analysis. The changes due to both the changes of the conformation of the molecules, its species, nonionic neutral versus zwitterionic neutral, and also the solvent environment further complicate both the spectral simulations, but also the analysis of the experimental spectra and the changes which occur as one perturbs the system. The perturbations we make are relatively straightforward conceptually: temperature, pressure, volume and concentration. But in the diseased state of biomolecules in our bodies, the systems are even more complex. There is a wealth of experimental data which is increasing every day. But to be able to model and understand such spectra and spectral changes, we have had to make major advances and breakthroughs in biomolecular spectroscopic modeling. Our work here is but one small step to achieving that long term worthy goal.

Acknowledgments We would like to acknowledge scientific discussions with the following collaborators and friends: Daniel Chipman, Victor Ya. Artyukhov for common discussions concerning theoretical questions and methodology; John S. Tse and Dennis D. Klug for initial discussions concerning the properties of cyanoanthracene; and Yuriko Aoki for discussions of benzene and estradiol. We would also like to thank the following funding agencies and institutions for supporting this work during its various stages of development: Kyushu University, Japan; Steacie Institute for Molecular Sciences, Canada; University of Notre Dame, USA; Siberian Physical-Technical Institute, Russia; Siberian Federal University, Russia; Kirensky Institute of Physics, Russia. We would like to thank FAPESP for project 16782-2/2009 which allowed Prof. Jalkanen to visit LEVB at UniVaP for the period from June 2010 to May 2011 from the Quantum Protein (QuP) Center at the Technical University in Denmark during which time this work was completed.

References

1. Atkins PW, Friedman RS (2010) Molecular quantum mechanics, 5th edn. University Press, Oxford
2. Jensen F (2007) Introduction to computational chemistry. Wiley, London
3. Frenkel D (1996) Understanding molecular simulation. Academic Press, Orlando
4. Car R, Parrinello M (1985) Unified approach for molecular dynamics and density-functional theory. Phys Rev Lett 55:2471–2474
5. Kühne TD, Krack M, Mohamed FR, Parrinello M (2007) Efficient and accurate car-parrinello-like approach to Born-Oppenheimer molecular dynamics. Phys Rev Lett 98:066401
6. Pomogaev V, Pomogaeva A, Aoki Y (2009) Absorption spectra of estradiol and tryptophan constructed by the statistical and elongation methods. J Phys Chem A 113:1429–1433
7. Artyukhov VYa, Maier GV (2001) Quantum-chemical theory of electronic excitation energy transfer in molecular systems. Russ J Phys Chem 75:1034–1040, ISSN 0036-0244. http://elibrary.ru/item.asp?id=13384997
8. Pomogaev VA (2002) T → S Energy transfer in some molecular complexes. High Energy Chem 36:250–254, doi:10.1023/A:1016273322998
9. Pomogaev VA, Artyukhov VY (2002) Quantum-chemical study of spectral-luminescent properties of indole. Atmos Oceanic Opt 15:213–216, ISSN 0235-6880/02/03. http://ao.iao.ru/en/content/vol.15-2002/iss.03/?&annot=16
10. Pomogaev V, Gu FL, Pomogaeva A, Aoki Y (2009) Elongation method for calculating excited states of aromatic molecules embedded in polymers. Int J Quantum Chem 109:1328–1340
11. He L, Li H, Fan J, Li S, Gan Q, Zhang G, Zhang B, Li Y, Yang G (2003) High pressure effect on the intramolecular electron transfer process. Chem Phys Lett 378:263–268
12. Jalkanen KJ (2003) Energetics, structures, vibrational frequencies, vibrational absorption, vibrational circular dichroism and Raman intensities of Leu-enkephalin. J Phys Condens Matter 15:S1823–S1851
13. Nikiforovich GV, Balodis J (1988) A model for the δ-receptor-bound conformation of enkephalin. FEBS Lett 227:127–130
14. Abdali S, Niehaus TA, Jalkanen KJ, Cao X, Nafie LA, Frauenheim T, Suhai S, Bohr H (2003) Vibrational absorption spectra, DFT and SCC-DFTB conformational study and analysis of Leu-enkephalin. Phys Chem Chem Phys 5:1295–1300
15. Jalkanen KJ, Elstner M, Suhai S (2004) Amino acids and small peptides as building blocks for proteins: comparative theoretical and spectroscopic studies. J Mol Struct 675:61–77
16. Jalkanen KJ, Jurgensen VW, Claussen A, Rahim A, Jensen GM, Wade RC, Nardi F, Jung C, Degtyarenko IM, Nieminen RM, Herrmann F, Knapp-Mohammady M, Niehaus TA, Frimand K, Suhai S (2006) The use of vibrational spectra to study protein and DNA structures, hydration, and binding of biomolecules: a combined theoretical and experimental approach. Int J Quantum Chem 106:1160–1198
17. Young D (2001) Computational chemistry. Wiley-Interscience. Appendix A. A.2.4 pg 336. Gaussian. [http://www.gaussian.com/g_tech/g_ur/m_citation.htm]
18. http://www-theor.ch.cam.ac.uk/software/cadpac.html
19. Young D (2001) Computational chemistry. Wiley-Interscience. Appendix A. A.2.1 pg 332, ADF. [http://www.scm.com/]
20. http://www.turbomole.com/
21. http://www.kjemi.uio.no/software/dalton/
22. http://accelrys.com/products/materials-studio/
23. Gordon MS, Schmidt MW (2005) In: Dykstra CE, Frenking G, Kim KS, Scuseria GE (eds) Theory and applications of computational chemistry: the first forty years. Elsevier, Amsterdam. GAMESS (Mar 2007), http://www.msg.ameslab.gov/GAMESS
24. Lazzeretti P, Zanasi R (1986) Electric and magnetic nuclear shielding tensors: a study of the water molecule. Phys Rev A 33:3727–3741
25. Lazzeretti P, Zanasi R (1987) Electromagnetic nuclear shielding tensors and their relation to other second-order properties. A study of the methane molecule. J Chem Phys 87:472–480
26. Karlström G, Lindh R, Malmqvist P-Å, Roos BO, Ryde U, Veryazov V, Widmark P-O, Cossi M, Schimmelpfennig B, Neogrady P, Seijo L (2003) MOLCAS: a program package for computational chemistry. Comp Mat Sci 28:222–239
27. Kresse G, Furthmüller J (1996) Efficient iterative schemes for ab initio total-energy calculations using a plane-wave basis set. Phys Rev B 54:11169–11186
28. Soler JM, Artacho E, Gale JD, Garcıa A, Junquera J, Ordejon P, Sanchez-Portal D (2002) The SIESTA method for ab initio order-N materials simulation. J Phys Condens Matter 14:2745–2779, http://www.icmab.es/siesta/
29. Roothaan CCJ (1951) New developments in molecular orbital theory. Rev Mod Phys 23:69–89

30. Hall GG (1951) The molecular orbital theory of chemical valency. VIII. A method of calculating ionization potentials. Proc R Soc Lond Ser A 205:541–552, http://www.jstor.org/pss/98703
31. Møller C, Plesset MS (1934) Note on an approximation treatment for many-electron systems. Phys Rev 46:618–622
32. Head-Gordon M, Pople JA, Frisch MJ (1988) MP2 energy evaluation by direct methods. Chem Phys Lett 153:503–506
33. Cramer CJ (2004) Including electron correlation in molecular orbital theory. In Essentials of computational chemistry, 2nd edn. Wiley, Chichester, pp 203–248, ISBN: 978-0-470-09182-1
34. Roos BO, Andersson K, Fülscher MP, Malmqvist PÅ, Serrano-Andrés L, Pierloot K, Merchán M (2006) Multiconfigurational perturbation theory: applications in electronic spectroscopy. In: Prigogine I, Rice SA (eds) Advances in chemical physics: new methods in computational quantum mechanics, vol XCIII. Wiley, New York, pp 219–331
35. Dewar MJS, Zoebisch EG, Healy EF, Stewart JJP (1985) AM1: a new general purpose quantum mechanical molecular model. J Am Chem Soc 107:3902–3909
36. Stewart JJP (2007) Optimization of parameters for semiempirical methods V: modification of NDDO approximations and application to 70 elements. J Mol Model 13:1173–1213
37. Kohn W, Sham L (1965) Self-consistent equations including exchange and correlation effects. Phys Rev A 140:1133–1138
38. Koch W, Holthausen MC (2002) A chemist's guide to density functional theory. Wiley-VCH, Weinheim
39. Thomas LH (1927) The calculation of atomic fields. Proc Cambridge Philos Soc 23:542–548
40. Fermi E (1927) Un metodo statistico per la determinazione di alcune priorieta dell'atome'. Rend Accad Naz Lincei 6:602–607
41. Gerasimov SA, Zhdanova EI (1986) Inelastic scattering of charged particles by atoms using the Thomas-Fermi statistical method. Russ J Phys 29:765–768. doi:10.1007/BF00895470
42. Dirac PAM (1930) Note on exchange phenomena in the Thomas-Fermi atom. Proc Cambridge Philos Soc 26:376–385
43. Gusarov S, Malmqvist P-Å, Lindh R, Roos BO (2004) Correlation potentials for a multi-configurational based density functional theory with exact exchange. Theor Chem Acc 112:84–94
44. Gräfenstein J, Cremer D (2005) Development of a CAS-DFT method accounting for non-dynamical and dynamical electron correlation in a balanced way. Mol Phys 103:279–308
45. Bartlett RJ, Schweigert IV, Lotrich VF (2006) Getting the right answer for the right reason. J Mol Struct THEOCHEM 771:1–8
46. Jalkanen KJ, Suhai S (1996) N-Acetyl-L-alanine N'-methylamide: a density functional analysis of the vibrational absorption and vibrational circular dichroism spectra. Chem Phys 208: 81–116
47. Jalkanen KJ, Bohr H, Suhai S (1997) Density functional and neural network analysis: hydration effects and spectroscopic and structural correlations in small peptides and amiono acids. In: Theoretical and computational methods in genome research. Plenum Press, pp 255–277
48. Ireta J, Neugebauer J, Scheffler M (2004) On the accuracy of DFT for describing hydrogen bonds: dependence on the bond directionality. J Phys Chem A 108:5692–5698
49. Lacks DJ, Gordon RG (1993) Pair interactions of rare-gas atoms as a test of exchange-energy-density functionals in regions of large density gradients. Phys Rev A 47:4681–4690
50. Lotrich VF, Bartlett RJ, Grabowski I (2005) Intermolecular potential energy surfaces of weakly bound dimers computed from ab initio density functional theory: the right answer for the right reason. Chem Phys Lett 405:43–48
51. Gerber IC, Ángyán JG (2005) Potential curves for alkaline-earth dimers by density functional theory with long-range correlation corrections. Chem Phys Lett 416:370–375
52. Zhao Y, Truhlar DG (2006) Comparative DFT study of van der Waals complexes: Rare-Gas Dimers, Alkaline-Earth Dimers, Zinc Dimer, and Zinc-Rare-Gas dimers. J Phys Chem A 110:5121–5129
53. Amos RD (1984) Dipole moment derivatives of H_2O and H_2S. Chem Phys Lett 108:185–190
54. Stephens PJ (1985) Theory of vibrational circular dichroism. J Phys Chem 89:748–752
55. Johnson BG, Florián J (1995) The prediction of Raman spectra by density functional theory. Preliminary findings. Chem Phys Lett 247:120–125
56. Amos RD (1986) Calculation of polarizability derivatives using analytic gradient methods. Chem Phys Lett 124:376–381
57. Han WG, Jalkanen KJ, Elstner M, Suhai S (1998) Theoretical study of Aqueous *N*-Acetyl-L-alanine *N*'-Methylamide: structures and Raman, VCD, and ROA spectra. J Phys Chem B 102:2587–2602
58. Jalkanen KJ, Nieminen RM, Bohr J (2000) Simulations and analysis of the Raman scattering and differential Raman scattering/Raman optical activity (ROA) spectra of amino acids, peptides and proteins in aqueous solution. Vestnik Moskovskogo Universiteta. Khimiya 41:4–7, http://www.chem.msu.su/eng/journals/vmgu/00add/4.pdf
59. Jalkanen KJ, Nieminen RM, Frimand K, Bohr J, Bohr H, Wade RC, Tajkhorshid E, Suhai S (2001) A comparison of aqueous solvent models used in the calculation of the Raman and ROA spectra of L-alanine. Chem Phys 265:125–151
60. Yurenev PV, Shcherbinin AV, Stepanov NF (2010) The applicability of TD-DFT methods to calculations of the electronic absorption spectrum of hexaamminoruthenium(II) in aqueous solution. Russ J Phys Chem A 84:39–43, doi:10.1134/S0036024410010085
61. Dreuw A, Head-Gordon M (2005) Single-reference ab initio methods for the calculation of excited states of large molecules. Chem Rev 105:4009–4037
62. Day PN, Jensen JH, Gordon MS, Webb SP, Stevens WJ, Krauss M, Garmer D, Basch H, Cohen D (1996) An effective fragment method for modeling solvent effects in quantum mechanical calculations. J Chem Phys 105:1968–1986
63. Pecul M, Ruud K, Helgaker T (2004) Density functional theory calculation of electronic circular dichroism using London orbitals. Chem Phys Lett 388:110–119
64. Thorvaldsen AJ, Ruud K, Kristensen K, Jørgensen P, Coriani S (2008) A density matrix-based quasienergy formulation of the Kohn–Sham density functional response theory using perturbation- and time-dependent basis sets. J Chem Phys 129:214108
65. Shcherbin D, Ruud K (2008) The use of Coulomb-attenuated methods for the calculation of electronic circular dichroism spectra. Chem Phys 349:234–243
66. Jacquemin D, Perpète EA, Scalmani G, Frisch MJ, Assfeld X, Ciofini I, Adamo C (2006) Time-dependent density functional theory investigation of the absorption, fluorescence, and phosphorescence spectra of solvated coumarins. J Chem Phys 125:164324
67. Improta R, Scalmani G, Frisch MJ, Barone V (2007) Toward effective and reliable fluorescence energies in solution by a new state specific polarizable continuum model time dependent density functional theory approach. J Chem Phys 127:074504
68. Autschbach J (2007) Density functional theory applied to calculating optical and spectroscopic properties of metal complexes: NMR and optical activity. Coord Chem Rev 251: 1796–1821
69. Solans-Monforta X, Eisenstein O (2006) DFT calculations of NMR J_{C-H} coupling constants: An additional tool to characterize the α-agostic interaction in high oxidation state M-alkylidene complexes (M = Re, Mo and Ta). Polyhedron 25:339–348

70. Lee AM, Handy NC, Colwell SM (1995) The density functional calculation of nuclear shielding constants using London atomic orbitals. J Chem Phys 103:10095–10109
71. Gester RM, Georg HC, Canuto S, Caputo MC, Provasi PF (2009) NMR Chemical Shielding and Spin-Spin Coupling Constants of Liquid NH_3: A Systematic Investigation using the Sequential QM/MM Method. J Phys Chem A 113:14936–14942
72. Aidas K, Mikkelsen KV, Kongsted J (2010) On the existence of the H3 tautomer of adenine in aqueous solution. Rationalizations based on hybrid quantum mechanics/molecular mechanics predictions. Phys Chem Chem Phys 12:761–768
73. Buckingham AD, Fowler PW, Galwas PA (1987) Velocity-dependent property surfaces and the theory of vibrational circular dichroism. Chem Phys 112:1–14
74. Webster FA, Friedrichs MS, Friesner RA, Rossky PJ (1991) Solvation dynamics of the hydrated electron: a nonadiabatic quantum simulation. Phys Rev Lett 66:3172–3175
75. Nicolas C, Boutin A, Levy B, Borgis D (2003) Molecular simulation of a hydrated electron at different thermodynamic state points. J Chem Phys 118:9689–9696
76. Shkrob IA, Glover WJ, Larsen RE, Schwartz BJ (2007) The structure of the hydrated electron. Part 2. A mixed quantum/classical molecular dynamics embedded cluster density functional theory: single − excitation configuration interaction study. J Phys Chem A 111:5232–5243
77. Mochizuki Y, Komeiji Y, Ishikawa T, Nakano T, Yamataka H (2007) A fully quantum mechanical simulation study on the lowest n–π* state of hydrated formaldehyde. Chem Phys Lett 437:66–72
78. Ludwig V, Coutinho K, Canuto S (2004) Sequential classical-quantum description of the absorption spectrum of the hydrated electron. Phys Rev B 70:214110
79. Mortin ME, Losa AM, Fdez-Galvan I, Aguilar MA (2004) A theoretical study of solvent effects on the 1(n $\rightarrow$ π^*) electron transition in acrolein. J Chem Phys 121:3710–3716
80. Georg HC, Coutinho K, Canuto S (2005) A sequential Monte Carlo quantum mechanics study of the hydrogen-bond interaction and the solvatochromic shift of the n–π* transition of acrolein in water. J Chem Phys 123:124307
81. Georg HC, Coutinho K, Canuto S (2007) Solvent effects on the UV-visible absorption spectrum of benzophenone in water: a combined Monte Carlo quantum mechanics study including solute polarization. J Chem Phys 126:034507
82. Besley NA, Oakley MT, Cowan AJ, Hirst JD (2004) A sequential molecular mechanics/quantum mechanics study of the electronic spectra of amides. J Am Chem Soc 126:13502–13511
83. Raynaud C, Poteau R, Maron L, Jolibois F (2006) Ab initio molecular dynamics simulation of the UV absorption spectrum of β-ionone. 771:43–50
84. Yoo S, Zahariev F, Sok S, Gordon MS (2008) Solvent effects on optical properties of molecules: a combined time-dependent density functional theory/effective fragment potential approach. J Chem Phys 129:144112
85. Arora P, Slipchenko LV, Webb SP, DeFusco A, Gordon MS (2010) Solvent-induced frequency shifts: configuration interaction singles combined with the effective fragment potential method. J Phys Chem A 114:6742
86. Virshup AM, Punwong C, Pogorelov TV, Lindquist BA, Ko C, Martınez TJ (2009) Photodynamics in complex environments: ab initio multiple spawning quantum mechanical/molecular mechanical dynamics. J Phys Chem B 113:3280–3291
87. Osted A, Kongsted J, Mikkelsen KV, Åstrand PO, Christiansen O (2006) Statistical mechanically averaged molecular properties of liquid water calculated using the combined coupled cluster/molecular dynamics method. J Chem Phys 124:124503
88. Wu Y, Tepper HL, Voth GA (2006) Flexible simple point-charge water model with improved liquid-state properties. J Chem Phys 124:024503
89. Jalkanen KJ, Degtyarenko IM, Nieminen RM, Cao X, Nafie LA, Zhu F, Barron LD (2008) Role of hydration in determining the structure and vibrational spectra of L-alanine and *N*-acetyl L-alanine *N*'-methylamide in aqueous solution: a combined theoretical and experimental study. Theor Chem Acc 119:191–210
90. Degtyarenko IM, Jalkanen KJ, Gurtovenko AA, Nieminen RM (2007) L-alanine in a droplet of water: a first principle molecular dynamics study. J Phys Chem B 111:4227–4234
91. Gaigeot MP, Sprik M (2003) Ab Initio molecular dynamics computation of the infrared spectrum of aqueous uracil. J Phys Chem B 107:10344–10358
92. Gaigeot MP, Sprik M (2004) Ab Initio molecular dynamics study of uracil in aqueous solution. J Phys Chem B 108:7458–7467
93. Bowler DR, Miyazaki T, Gillan MJ (2002) Recent progress in linear scaling ab initio electronic structure techniques. J Phys Condens Matter 14:2781–2798
94. Olsen JM, Aidas K, Mikkelsen KV, Kongsted J (2010) Solvatochromic shifts in uracil: a combined MD-QM/MM study. J Chem Theory Comput 6:249–256
95. Kalkman I, Brand C, Vu T-BC, Meerts WL, Svartsov YN, Dopfer O, Tong X, Müller-Dethlefs K, Grimme S, Schmitt M (2009) The structure of phenol-Arn (n = 1, 2) clusters in their S0 and S1 states. J Chem Phys 130:224303
96. Häber T, Seefeld K, Engler G, Grimme S, Kleinermanns K (2008) IR/UV spectra and quantum chemical calculations of Trp-Ser: stacking interactions between backbone and indole side-chain. Phys Chem Chem Phys 10:2844–2851
97. Guthmuller J, Zutterman F, Champagne B (2009) Multimode simulation of dimer absorption spectra from first principles calculations: application to the 3, 4, 9, 10-perylenetetracarboxylic diimide dimer. J Chem Phys 131:154302
98. Zerner M (1991)Semiempirical molecular orbital methods. In: Lipkowitz KB, Boyd DB (eds) Reviews in computational chemistry, vol 2. VCH, New York, pp 313–365, doi:10.1002/9780470125793.ch8
99. McGlynn C, Azumi T, Kinosita M (1969) Molecular spectroscopy of the triplet state. Prentice-Hall, New Jersey
100. Artykhov VYa, Pomogaev VA (2000) Three-center integrals of one-electron operator of a spin-orbit interaction. Russ Phys J 4:590–600, doi:10.1007/BF02508964
101. Iwata T, Hirose T, Yamaguchi M (1997) Direct determination of estriol 3- and 16-glucuronides in pregnancy urine by column-switching high-performance liquid chromatography with fluorescence detection. J Chromatogr B 695:201–207
102. Edman K, Svensson L, Eriksson B, Gunnarsson PO (2000) Determination of estramustine phosphate and its metabolites estromustine, estramustine, estrone, and estradiol in human plasma by liquid chromatography with fluorescence detection and gas chromatography with nitrogen-phosphorus and mass spectrometric detection. J Chromatogr B 738:267–279
103. Meshalkin YP, Cherkasova OP, Fedorov VI, Samoilova ES (2002) Laser-induced fluorescence of estrogens. Opt Spectrosc 92:32–35, doi:10.1134/1.1446579
104. Meshalkin YP, Artyukhov VY, Pomogaev VA (2003) Optical properties of two types of sex hormones of the cyclopentenephenanthrene series. Opt Spectrosc 95:377–380, doi: 10.1134/1.1612998
105. Philis J, Bolovinos A, Andritsopoulos G, Pantos E, Tsekeris P (1981) A comparison of the absorption spectra of the fluorobenzenes and benzene in the region 4.5–9.5 eV. J Phys B 14:3621–3635
106. Gentle IR, Ritchie GLD (1989) Second hyperpolarizabilities and static and optical-frequency polarizability anisotropies of

benzene, 1, 3, 5-trifluorobenzene and hexafluorobenzene. J Phys Chem 93:7740–7744
107. Hiraya A, Shobatake K (1991) Direct absorption spectra of jet-cooled benzene in 130–260 nm. J Chem Phys 94:7700–7706
108. Deleuze MS, Trofimov AB, Cederbaum LS (2001) Valence one-electron and shake-up ionization bands of polycyclic aromatic hydrocarbons. I. Benzene, naphthalene, anthracene, naphthacene, and pentacene. J Chem Phys 115:5859–5882
109. Du H, Fuh RA, Li J, Corkan A, Lindsey JS (1998) PhotochemCAD: a computer-aided design and research tool in photochemistry. Photochem Photobiol 68:141–142, http://omlc.ogi.edu/spectra/PhotochemCAD/html/du98.html
110. TINKER—Software Tools for Molecular Design, http://dasher.wustl.edu/tinker/
111. CCLRC Computational Science and Engineering Department, DLPOLY, http://www.cse.clrc.ac.uk
112. Lii JH, Allinger NL (1989) Molecular mechanics. The MM3 force field for hydrocarbons. 3. The van der Waals' potentials and crystal data for aliphatic and aromatic hydrocarbons. J Am Chem Soc 111:8576–8582
113. Tanaka H, Nakanishi K, Watanabe N (1983) Constant temperature molecular dynamics calculation on Lennard-Jones fluid and its application to water. J Chem Phys 78:2626–2634
114. Cornell WD, Cieplak P, Bayly CI, Gould IR, Merz KM, Ferguson DM, Spellmeyer DC, Fox T, Caldwell JW, Kollman PA (1995) A second generation force field for the simulation of proteins, nucleic acids, and organic molecules. J Am Chem Soc 117:5179–5197
115. Lin H, Hunter JA, Pfab J (1993) Laser-induced fluorescence spectroscopy of jet-cooled 2-methylanthracene S1 (π, π^*). Evidence for methyl conformation change upon electronic excitation. Chem Phys Lett 210:38–44
116. Hirayama S (1986) A comparative study of the fluorescence lifetimes of 9-cyanoanthracene in a bulb and supersonic free jet. J Chem Phys 85:6867–6873
117. Maple JR, Hwang M-J, Jalkanen KJ, Stockfisch TP, Hagler AT (1998) Derivation of class II force fields: quantum force field for amides, peptides, and related compounds. J Comp Chem 19:430–458